Final Draft
of the original manuscript:

Blawert, C.; Fechner, D.; Hoeche, D.; Heitmann, V.; Dietzel, W.; Kainer, K.U.; Zivanovic, P.; Scharf, C.; Ditze, A.; Groebner, J.; Schmid-Fetzer, R.:

Magnesium secondary alloys: Alloy design for magnesium alloys with improved tolerance limits against impurities

In: Corrosion Science (2010) Elsevier

DOI: 10.1016/j.corsci.2010.03.035

Magnesium secondary alloys:
Alloy design for magnesium alloys with improved tolerance limits against impurities

C.Blawert, D. Fechner, D. Höche, V. Heitmann, W. Dietzel and K.U. Kainer
GKSS Forschungszentrum Geesthacht GmbH
Max-Planck-Str. 1
21502 Geesthacht
Germany

P. Živanović, C. Scharf, A. Ditze, J. Gröbner, R. Schmid-Fetzer
TU Clausthal
Institut für Metallurgie
Robert-Koch-Str. 42
38678 Clausthal-Zellerfeld
Germany

1 Abstract

The development of secondary magnesium alloys requires a completely different concept compared with standard alloys which obtain their corrosion resistance by reducing the levels of impurities below certain alloy and process depending limits. The present approach suitable for Mg-Al based cast and wrought alloys uses a new concept replacing the ß-phase by τ-phase, which is able to incorporate more impurities while being electrochemically less detrimental to the matrix. The overall experimental effort correlating composition, microstructure and corrosion resistance was reduced by using thermodynamic calculations to optimise the alloy composition. The outcome is a new, more impurity tolerant alloy class with a composition between the standard AZ and ZC systems having sufficient ductility and corrosion properties comparable to the high purity standard alloys.

Keywords: magnesium A, secondary alloy A, intermetallics A, weight loss B, hydrogen overpotential C

Corresponding author: C. Blawert
GKSS Forschungszentrum Geesthacht GmbH
Max-Planck-Str. 1
21502 Geesthacht
Germany
Tel.: +49 4152 87 1991
Fax: +49 4152 87 2660
e-mail: carsten.blawert@gkss.de

2 Introduction

Today the awareness of environmental issues and problems is growing in the public and there is a general agreement that the CO_2 emission has to be reduced. However, magnesium alloys are often considered as “green” materials in transport applications offering the possibility to save energy and reduce CO_2 emission by saving weight of the vehicles and therefore reduce the fuel consumption. Thereby the energy consumption for producing the metal from the raw material (ore or salt) is often ignored. If the whole life cycle is considered, it can be essential that the light weight magnesium components are predominantly produced from secondary Mg alloys to reach the CO_2 balance in the average life time of a car as early as possible. Reducing the fuel consumption by light weight construction replacing aluminium and/or steel alone may not be sufficient. The use of secondary instead of primary magnesium alloys requires only a fraction of energy compared with primary magnesium production [1]. Thus life cycle assessment [2-6] reveals that magnesium is only a “green” metal if a considerable large amount of secondary magnesium is used, but recycling of magnesium post consumer scrap is not performed on the industrial scale and no defined secondary magnesium alloys comparable to aluminium secondary alloys such as A380 are available. The main reason for this is the possible up-take of heavy metal impurities during the recycling process with extremely detrimental effects on the corrosion resistance, but environmental and even economical issues require the development of secondary magnesium alloys.

Up to date, recycling of Mg is restricted to the re-melting of pure scrap (class 1) and of larger components which can be easily separated or cleaned from contaminations and sorted by the different alloys. If the impurity level during re-melting gets too high the melt will be blended with primary alloys to comply with the standard composition requirements. This is mainly done to keep the impurity level of heavy metals such as Cu, Ni, Co and Fe low and thus to guarantee a reasonable corrosion resistance of the standard Mg alloys. The impurity metals are part of standard scrap fractions, alloying elements in other light metals or are even used as coatings on Mg alloys, thus they can contaminate Mg alloys during the re-melting process if they are not completely removed from the scrap fraction. Because this is almost impossible and melt cleaning is difficult and expensive no used magnesium scrap (from shredder or dismantling) or coated (Ni, Cu) waste is really recycled up to now, in spite of the benefits mentioned above [7].

However, the use of secondary magnesium alloys is an essential step for the wide-spread use and acceptance of magnesium as a construction material, thus a joint project between the TU Clausthal and GKSS Forschungszentrum Geesthacht GmbH was started and funded by the DFG to develop such a secondary alloy five years ago.

Considering the overall magnesium alloy production volume, the alloy AZ91 is the most commonly used alloy and consequently the content of AZ in a scrap fraction can be expected to be relatively high. An additional prerequisite was the fact that a secondary alloy should be cheap thus no expensive additional alloying elements should be used. Therefore the first secondary magnesium alloy was developed based on the AZ system which was modified to tolerate higher levels and fluctuations of typical impurities only by optimising the microstructure and the composition [8, 9]. In a first step the Al content was increased to increase the volume of ß-phase and guarantee a dense ß-phase network formation for a large variety of casting conditions. However, by first screening corrosion tests it became obvious that increasing the Al content alone is not sufficient [10, 11]. Furthermore, the Al_8Mn_5 phase was identified to be the only phase that incorporates some nickel, thus it was obvious that a reasonable amount of Mn in the alloy was needed to address the Ni problem. Copper however was found in a variety of intermetallic phases while the negative effect on the corrosion resistance was found to increase with increasing Cu content in the phases [12, 13]. Interestingly, copper and zinc were found often in the same phases. This suggested that a Zn addition might be beneficial to promote phases which are able to incorporate Cu. From thermodynamic calculations it was obvious that considering the volume of the various phases only two phases are of interest to modify the microstructure. The ß-phase should form the corrosion barrier, while the τ-phase should incorporate the copper and prevent formation of more detrimental copper rich phases. Although the calculations suggest that 2 wt% of Zn are sufficient, an alloy with 3 wt% Zn was selected to reach more tolerance against variations in the copper content as well as variations in the casting conditions especially cooling rates. Corrosion tests revealed that the resulting alloy AZC1231 tolerated up to 0.5 wt% copper under various casting conditions (gravity die casting, semi-solid processing as well as high pressure die casting) having still corrosion rates comparable to AZ91D. The correlation of microstructure with corrosion rate and corrosion mechanisms suggests that for this alloy quite a number of different

mechanisms are responsible for improving the tolerance limits. The new alloy forms the intended ß-phase network around the grains. A grain refinement caused by the addition of Al, Zn and Mn makes it easier to form a dense network improving the barrier properties. Iron and nickel are incorporated by Al_8Mn_5 phase and copper by the τ-phase. Furthermore, ß and τ-phase are embedding other nobler and therefore critical precipitates, isolating them from a direct contact with the matrix, thus reducing galvanic effects. The ß-phase as the dominating phase is also embedding the τ-phase to a large extent [8-14].

In spite of good castability, strength and corrosion properties of the new alloy, suggesting that this alloy may offer a suitable alternative for many casting applications, it can not be used in applications were sufficient ductility is required [11, 14]. For wrought processing or more ductile cast applications an additional secondary magnesium alloy group is required. Such a development is by far a larger challenge than the alloy design for the AZC1231 alloy as the alloying element content has to be reduced for ductility reasons and thus the concept of using the ß-phase as a corrosion barrier and embedding agent for nobler precipitates is not available anymore. The demands for having sufficient scrap metal volume available and for the alloy itself to provide sufficient ductility lead our focus on the AM50 system.

However, it is well known that the ß($Mg_{17}Al_{12}$)-phase in AZ based alloys is cathodic to the matrix [15-17] and can either enhance or decrease the corrosion of the alloy depending on the distribution of the ß-phase [17-22]. If it is uniformly distributed at the grain boundaries, covering the whole grains and forming a dense network, it works as a corrosion barrier and improves the corrosion resistance of the alloy remarkably. However in AZ91D this beneficial ß-phase network forms only under certain casting conditions as the alloy content is on the lower level for forming a sufficient amount of ß-phase allowing the network to form. In AM50 alloy the Al level is much lower and mainly single separate ß-phase precipitates exist. Due to the much more noble character of the ß-phase compared with the Mg matrix, separated ß-phase precipitates in the matrix can cause localised galvanic corrosion and enhance the corrosion rate [23-25]. Thus the challenge was to develop a low aluminium containing alloy with sufficient ductility and tolerance against impurities without having the barrier function of a ß-phase network.

In the following the new alloy design concept and approach is introduced in more details. To reduce the experimental effort modelling of phase fractions as a function

of the alloy content was used. Finally the new alloy and its properties are introduced and the advantages are discussed.

3 Experimental

3.1 Casting

3.1.1 Single phases and/or intermetallics

For the galvanic corrosion testing typical phases in the Mg-Al-Zn-Cu system were prepared as single phases. The selection of the phases is mainly based on the microstructural characterisations performed during the development of the AZC1231 alloy in which three main phases were identified which can be used to modify the microstructure in an extent to have a major influence on the corrosion behaviour (α-matrix, β- and τ-phase). The amount of other intermetallics (e.g. Al_8Mn_5, $Al_{11}Mn_4$, Mg_2Cu, $MgCu_2$, $Al_7Cu_3Mg_6$ etc.) is either too low or the negative effects on the corrosion resistance are so high that their formation has to be prevented anyway. If not otherwise mentioned the selected compositions are typical, average compositions of the three phases determined in the microstructure of real castings by EDX analysis. According to the analysis the magnesium matrix is able to keep up to 15 wt% Al in solid solution. However, due to the fact that the average values were lower and due to the requirement that single phases are needed to represent the matrix in the galvanic coupling the Al content was limited to 3 and 6 wt%. The single phases were finally produced by solution treatment (24 h at 415°C) and quenching in water to prevent formation of ß-phase. The ß-phase as well as the τ-phase in the real microstructure are able to incorporate other alloying elements and impurities. Thus, Zn and small amounts of Cu can be found in the ß-phase (Mg-Al intermetallic) and the τ-phase (Mg-Al-Zn intermetallic) can replace obviously Zn by Cu without changing its structure. This finding is reflected by selecting pure ß-phase, ß-phase with 5 wt% Zn, pure τ-phase and τ-phase with Cu for the electrochemical compatibility studies. The elemental compositions of the casted single phases are given in Table 1.

The weight fractions of pure Mg, Al, Zn and Cu according to the required composition were melted at 730°C followed by stirring for 30 minutes under protective atmosphere. After a short settling time of 10 minutes, the melts with quantities of 100

g each were poured into thick walled cylindrical steel dies of 16 mm diameter were the melt solidified quickly. Please note that all intermetallic specimens were tested intentionally in the as cast condition (not homogenized) with segregations, which is closer to the appearance of the real precipitates in the alloys. The microscopic validation including EDX revealed that only specimen Tau(Cu) consisted clearly of two different τ-phases, one was low and the other was high in copper content. The existence of copper rich and copper low τ-phases is consistent with the large solubility range predicted by thermodynamic calculations. Also the other intermetallic specimens were not 100% pure and contained small remains of Mg in the case of ß and Al in the case of τ as well as some minor iron impurities. The effect of the remains on the corrosion performance was considered as low, because Mg will dissolve rapidly and small Al and other nobler impurities will fall of the specimens due to galvanic enhanced dissolution of the matrix around them. The small concern regarding the purity of the specimens and its effect on the corrosion resistance is considered by clearly distinguishing between the specimens (labelled Beta, Beta(Zn), Tau and Tau(Cu)) and the respective phases (labelled β, β(Zn), τ, and τ(Cu)).

3.1.2 Secondary alloys

All castings of the secondary magnesium alloys (for phase analysis and determination of tolerance limits) were prepared from commercially available alloy AM50 as starting material. Alloys with nominal 5 wt% Al and 0-4 wt% Zn were melted having copper and nickel contents in the range of 0-2.0 wt% and of 0-0.22 wt% respectively. Zinc and the impurities were added to 1 kg of commercial alloys at a melt temperature between 680 and 730°C. The alloys were cast into bars of 30 mm diameter and 300 mm length by gravity die casting.

Two main sets of specimens were prepared to evaluate on the one hand the influence of Zn additions in the presence of impurities and on the other hand to determine the tolerance limits for the proposed secondary alloy AZ53. In the first case, the fact that a secondary alloy should be developed is considered by assuming higher Ni and Cu contents. The impurity contents of 32 – 45 ppm Ni or 0.5 wt% Cu were selected according to the acceptable impurity levels identified for the secondary alloy AZC1231 which are much higher than the standard allowance for high purity alloys. Iron is not considered as it is more appropriate to remove the iron by a melt treatment with manganese. In contrast, Ni and Cu are more difficult to be removed

from the melt, thus one has to find other ways to cope with these contaminations if a reasonable cheap secondary alloy should be available. In the second case increasing amounts of either Ni (up to 0.1 wt%) or Cu (up to 2 wt%) are added to the proposed pure secondary alloy AZ53.

The compositions of the castings were determined and controlled by solving the samples from each ingot in hydrochloric acid with subsequent recording of the emission by ICP-OES. The composition of all the alloys used in the present study is given in Table 1.

3.2 Prediction of phase fractions

An essential step in the present alloy development is to check the possibility to suppress the formation of ß-phase and promote formation of τ-phase in an alloy system that has a low Al content fulfilling the requirements of ductility. This can be done experimentally by casting various alloy compositions and determination of the obtained phases, but such an approach is expensive and time consuming. The faster and more science based approach is a thermodynamic calculation of the phase fractions after casting of modified AM50 alloys contaminated with copper. Nickel was not considered because the content should not exceed the ppm range due to its extremely negative effect on the corrosion resistance. This implies that no real effects on the phase fractions can be expected. Thus theoretical calculations of the solidification of the alloys as a function of various Zn contents at constant Cu (0.5 wt%), Mn (0.5 wt%) and Al (5 wt%) contents were performed using the Scheil model (no diffusion in the solid phases is assumed). All the calculations were performed using the PanMagnesium8 database and the Pandat software package [26].

3.3 Microstructure

Discs of 4 mm thickness and 25 mm diameter were cut from the ingots in the as cast condition for corrosion (immersion and salt spray) testing, metallographic inspection and phase analysis. The cross sections of the samples were ground with silicon carbide emery papers up to 2500 grit, and then polished with OPS™ lubricated with soapy deionised water. The surface of the polished samples were finally cleaned with ethanol and dried with warm flow air. If required the samples were etched with a mixture of picric acid, water and ethanol for the characterisation with light microscopy using polarised light. The prepared specimens were also studied by scanning electron microscopy (not etched). The analysis of the elements present in the phases

was performed by EDX. Additional information about the phases was obtained by X-ray diffraction using $\Theta/2\Theta$ mode and Cu-k_α radiation.

3.4 Corrosion testing

For all the corrosion tests the samples were ground with 1200 grit emery paper and rinsed with water and ethanol prior to the testing.

Information about the electrochemical behaviour of the single intermetallic phases was obtained by performing potentiodynamic polarization measurements in 5% NaCl solution, saturated with atmospheric oxygen. A typical three electrode cell (Ag/AgCl reference (with 3 mol/l KCl), Pt counter and the specimens as working electrode) was used. A starting pH of 11 was adjusted with NaOH and the temperature was controlled at 22 ± 0.5°C while stirring the electrolyte during the experiments. After 30 minutes recording of the free corrosion potential, the polarization scan was started from –200 mV relative to the free corrosion potential with a scan rate of 0.2 mV/s. The test was terminated when a corrosion current density of 0.1 mA/cm^2 was exceeded.

The galvanic corrosion susceptibility of the main phases in the AMZC alloy system (solid solution Mg phase (Mg with 0, 3 and 6 wt% Al), pure ß-phase, ß-phase with 5 wt% Zn, pure τ-phase and τ-phase with Cu) was checked by measuring the galvanic current between the various combinations of the phases. A corrosion cell with two specimens (surface size of 0.5 cm^2) facing each other in a distance of 50 mm and two Ag/AgCl reference electrodes for measuring the open circuit potentials of the two phases for 30 min before starting the test was used. At short circuit the mixed potential was only recorded by one of the reference electrodes and the current between the two specimens was measured using the zero resistance ampere meter setting of the potentiostat (Gill AC, ACM Instruments). The current was monitored for a total period of 20 hours. The electrolyte was the same as described above except that the volume in the cell was only 150 ml.

Additional information about the passive film formation on the surface was obtained from simple immersion test in deionized water (1 hour and 24 hours) and from electrochemical impedance spectroscopy (EIS) measurements performed in the same electrolyte and the same cell as described above for the polarisation measurements. Latter tests were performed at open circuit potential in the frequency

range of 0.1 to 10,000 Hz using amplitudes of ± 10 mV. The charge transfer resistances were simply taken at the intersection of the Nyquist Plot with the real axis (corrected by the solution resistance) representing the direct current ohmic resistance. The passive film formed on the immersion specimens was studied by XPS analysis performed with a Kratos Axis Ultra DLD. It works with Al K_α monochromatic radiation at 15 kV and a spherical lens detector. Experiments have been carried out at 10^{-9} bar using pass energies of 40 eV at region scans (bonding states) and of 160 eV at survey scans in order to determine chemical compositions. The spot size was 700x300 µm. Depth profiling and etching was performed by means of argon ion beam irradiation at currents up to 100 µA using a raster like scheme of 2x2 mm. According to calibration experiments the etching rates were assumed to be 25 or 36 nm/min. All experiments were carried out using a charge neutralizer attached at the measuring system. Latter is required because of the non conducting properties of $Mg(OH)_2$ and the resulting peak shifts due to charging effects if the neutralizer is not used. By means of survey scans the elemental compositions of the surface of the different alloy systems was determined using the evaluation software CasaXPS [27]. The depth profiles were measured by means of argon sputtering for 1000 s in 250 s steps.

Furthermore all alloy specimens were tested by automated immersion test and salt spray test. For the immersion test the specimens were immersed for more than 400 h into 1.9 l of 3.5% NaCl solution. The pH during immersion was kept at a constant value of pH6 by adding 0.025 m HCl. The corrosion rate was calculated from the amount of collected hydrogen. The salt spray tests were performed for 48 h according to DIN50021 with 5% NaCl solution (pH 6.5). The corrosion rates were determined from the weight loss of the specimens, after removing all the corrosion products using chromic acid. For defining the tolerance limit the corrosion performance of the modified and contaminated alloy AZ53 was compared with the performance of the standard alloy AM50 casted and tested under the same conditions. The tolerance limits by definition are the maximum possible impurity contents of Cu or Ni in the alloy AZ53 which can be added without exceeding the corrosion rate of the high purity AM50.

4 Methodology

The present alloy development for a secondary magnesium alloy is based on a number of prerequisites that such an alloy has to fulfil, addressing the performance as well as availability of scrap and economic aspects, namely:

1) Ductility which limits the Al content of the alloy to about 5 wt% but offers an alternative to the AZC1231 secondary alloy
2) Sufficient amount of scrap should be available, thus the alloy system should be based on AZ and AM based standard alloys because they are the most frequently used magnesium alloys
3) If possible no expensive additional alloying elements should be used because a secondary alloy must be cheaper than a standard alloy
4) Manganese should be used as an alloying element for reducing and controlling the iron impurity level
5) A positive effect of Zn on the corrosion resistance of Mg alloys in the presence of impurities was already noticed by Hanawalt et al. [27]
6) The alloy should have high Cu and Ni tolerance limits. Iron was not considered, because the iron content can be better controlled by manganese additions during melting [7]

Considering these prerequisites the alloying system is more or less fixed to an AM50 alloy modified with Zn. As explained in the introduction this has the consequence that the concept of using the ß-phase as a corrosion barrier and embedding agent for more noble precipitates is not available anymore. Therefore, another approach is required to optimise the corrosion resistance and increase the tolerance limit against impurities.

However, optimising the corrosion resistance of Mg alloys requires the knowledge of the phases present in the alloy, their phase fraction and distribution and finally their electro-chemical compatibility with the Mg matrix. Furthermore the content (phase fraction) of the phases in the alloy should be high enough to offer sufficient possibilities to manipulate their distribution, encapsulate other phases (intermetallics) and/or to incorporate larger amounts of impurities. The microstructural studies of the alloy AZC1231 [8-11, 14] clearly indicated that there are only three major phase fractions in the Mg-Al-Zn-System, namely Mg-Al solid solution, ß- and τ-phase, which can be used to actively influence the corrosion performance.

To the knowledge of the authors the electro-chemical properties of the τ-phase were unknown, while the properties of the Mg-Al solid-solution (α) matrix and the ß-phase were very well characterised [15-25, 28, 29]. Thus the first step in the alloy development was a study of the galvanic coupling of the τ-phase with α-matrix and with β-phase. The results indicated that the τ-phase is less detrimental to the matrix compared with the ß-phase (see 5.1.). Thus a new alternative approach appeared to be feasible in the Mg-Al-Zn system replacing ß-phase by τ-phase. At this stage thermodynamic calculations of the phase fractions after casting (Scheil model) were used to identify the optimum alloy composition according to the intention of maximising the τ-phase and minimising the β-phase fraction (see .5.2.). The modelling contemplated an AM50 base alloy with various Zn contents in the presence of 0.5 wt% Cu. After having identified the best suitable alloy composition (AZC531) the real microstructure was evaluated and compared with the predictions of the thermodynamic calculation (see 5.3.) followed by a validation of the ductility requirement (see 5.4.). The final step of the alloy development was the determination of the corrosion properties (see 5.5.) including the influence of Zn and the determination of the tolerance limits.

5 Results

5.1 Corrosion and galvanic corrosion properties of the main phases

A general step in improving the corrosion resistance of magnesium alloy is the understanding of the electrochemical interaction of the various intermetallic phases in the alloy in order to reduce the effect and amount of internal micro galvanic couples. Selected polarization curves of the four chosen intermetallic specimens are shown in Fig. 1a. It is obvious that the pure ß-phase is the less noble phase and therefore should be the most compatible phase with the matrix from the potential difference point of view. Adding 5 wt% Zn to the ß-phase shifts the potential to more noble values, without changing the corrosion resistance too much, but the extension of the passive region is reduced. The τ-phases have nobler potentials than the zinc containing ß-phase (called ß(Zn)) and the corrosion resistance is relatively low. Interestingly, the hydrogen evolution on the τ-phases is suppressed while being cathodically polarized and there is no indication of a passive region while being

anodically polarized. Among the two different Tau specimens the copper containing one (Tau(Cu)) is the least noble which can be correlated with the overall lower Zn content compared with the pure Tau specimen containing only the pure τ-phase without copper. The corrosion resistance of the pure τ-phase is only marginally improved in comparison with the τ-phase with joint solid solution of Zn and Cu of specimen Tau(Cu). The polarization curves for HP Mg and the two intermetallic specimens (Beta and Tau as an example) can be used to estimate the galvanic current between the Mg matrix and the two phases using the mixed potential theory (Fig. 1b). This suggests already that not the smallest potential difference of ß is the most determine parameter influencing the galvanic current in the couples, but the suppressed hydrogen formation on τ-phase.

This finding is confirmed by current measurements in real couplings of the selected intermetallic specimens with the matrix. In the case of τ the coupling results are only displayed for specimen Tau(Cu) as the solid solution of copper rich and copper low τ-phases is more comparable to the real appearance of τ-phase in the matrix of magnesium alloys. The results indicate a galvanic current that decreases in the following order: ß-phase with 5 wt%Zn > pure ß > τ (Fig. 2a). However this correlates very well with the retarded hydrogen evolution on the τ-phase while being cathodically polarized as shown in Fig. 1a and the prediction of the galvanic current by the mixed-potential method (Fig. 1b). The difference in galvanic current caused by pure τ-phase and solid solution of copper rich (called τ(Cu)) and low τ-phases is not large as shown in Tab. 2. It mainly follows the higher potential difference as the driving force of the galvanic current while the further increase in Zn causes obviously no further improvement in reducing the hydrogen generation. Thus the copper containing τ-phase τ(Cu) is less detrimental than the pure MgAlZn-τ-phase.

With increasing Al content in the matrix the current density measured against the various intermetallics is reduced (Fig. 2b and 2c). The increasing Al content is obviously beneficial for the corrosion resistance of the matrix and thus also reduces the galvanic current. The results are summarized in Tab. 2. It should be further noted that the galvanic current density between the various combinations of the intermetallic phases (ß, ß(Zn), τ(Cu) and τ) can be neglected. In any case the current density was found to be higher than 10 µA/cm^2.

5.2 Prediction of phase fractions

Due to the prerequisites introduced above the Al content was fixed to 5 wt% and practically the standard alloy AM50 was selected as the base for the modelling studies. The main target was an evaluation of the influence of Zn on the phase fractions of ß- and τ-phase in a contaminated alloy AM50. Only the influence of Cu impurities was considered as important for the microstructure of secondary alloys, because the nickel concentration in the ppm range can be neglected in this sense. Thus, the modelling examined only the effect of 0.5 wt% Cu addition as well as gradually increasing Zn contents from 0 to 5 wt%. A typical Scheil diagram for the alloy AZC531 is presented in Fig. 3 and the results of all calculations are summarized in Tab. 3 and 4.

With increasing zinc content the amount of α-phase (Mg-Al solid solution) is slightly reduced from 95.5% for pure AM50 to about 93.5% for AZC531 and 92% for AZC551. The total content of intermetallics in the alloys is correspondingly increasing from 4.5% to 6.5% and 8% respectively. This would suggest a drop in ductility with increasing Zn content, but especially for medium Zn contents sufficient ductility can be still expected. Beneficial for the intended improvement of the corrosion resistance is that the ß-phase content is reduced by the addition of Zn. The AM50 alloy contains about 4% of ß-phase while it is only about 1.7% for the AZC531 and 0.8% for AZC551 alloy. In the same manner the content of τ-phase is increasing from 0% (AM50) to about 3% for AZC531 and 3.5% for AZC551. Furthermore, there is also a contribution of Cu addition to the reduction of ß-phase and most likely to the increase of τ-phase as well if Cu and Zn are present concurrently. Important for an improved corrosion resistance is also the reduction of other detrimental phases. The Q-phase ($Al_7Cu_3Mg_6$) with high Al and Cu content is such a detrimental phase. It forms in AM50 based alloys if copper is added and reaches a content of about 1% for an AZC501 alloy. However if the Zn content has reached 3 wt% the Q-phase is completely suppressed. One has to note that the same can be observed for binary Mg_2Cu and $MgCu_2$ phases (experimentally found later but not part of the modelling). On the other hand the modelling suggests that new phases appear with increasing Zn content. There is the ε-phase (MgZn) with a phase fraction of 0.17% and 0.33% and the Φ-phase ($Mg_5Zn_2Al_2$) with 1.3% and 2.8% for the AZC531 and AZC551 alloys, respectively. This formation of new phases may have a detrimental influence on the corrosion resistance and may interfere with the beneficial effect of reducing

the ß-phase fraction and suppressing Q- and binary MgCu-phases. Therefore the results suggest that a Zn content of about 3 wt% could be a good choice.

The other important phase Al_8Mn_5 which is used to reduce and/or control the iron and nickel content during casting is only slightly influenced by the Zn additions. The content is increasing from 0.37% to about 0.43% for the higher Zn contents. The content of the other two Al_xMn_y compounds is reduced but the overall content is that low that detrimental effects are not expected.

Summarising, the idea of replacing ß- by τ-phase is theoretically possible, but there is no indication for a complete suppression of the ß-phase. Nevertheless there is sufficient theoretical evidence that the new concept may work and this has to be proven experimentally now. Based on the ductility requirement and the theoretically calculated phase fractions the most promising composition for a secondary alloy appears to be 5 wt% Al and 3 wt% Zn.

5.3 Real microstructure

The cross section micrographs in Fig. 4 show the influence of increasing Zn content (X = 0, 1 and 3 wt%) at a fixed Al content of 5 wt% on the microstructure of an AZC5X1 alloy containing 0.5 wt% Cu in comparison with the pure AM50 alloy. As expected, the overall amount of intermetallic phases is increasing with increasing Zn and Cu content, but they remain as single precipitates mainly along the grain boundaries without forming a dense network. The two main intermetallic phases are the ß- and the τ-phase. According to the Scheil calculation the amount of τ-phase is growing on the expense of the ß-phase if the Zn content in the alloy is increased. In the real microstructure the amount of τ-phase is increasing, but especially at the lower Zn content the reduction of ß-phase is not pronounced. However, estimating the phase fractions from the selected higher magnification micrographs is not accurate. Nevertheless, the reduction of the ß-phase fraction is obviously less than the increase of the τ-phase fraction which is again consistent with the Scheil calculations. There is another difference between calculation and real microstructure. The calculation is predicting no τ-phase for the alloy AZC501 while in the real microstructure a phase is detected which has a higher Cu content than the predicted Q-phase. We assume that this might be a ternary Mg-Al-Cu τ-phase and/or Mg-Al-Cu-Laves phases. However the most important finding is that the ß-phase is in none

of the alloys completely suppressed. Comparing the composition of precipitates in the alloy AZC501 and AZC531 reveals the other important role of the increasing Zn content [Tab. 6]. The precipitates in the Zn containing alloy have generally a much lower Cu content, which can be beneficial for the corrosion resistance (galvanic coupling). It is obvious that this transition is related to the formation of the quaternary Mg-Al-Zn-Cu τ-phase and most likely to the correlated reduction of Q-phase (according to Scheil calculation). The identified phases are suggesting that the system might be more complex, but it is very difficult to identify the phases based on the EDX analysis as most of them have overlapping solubility ranges and it can not be ruled out that surrounding and underlying phases are analysed together with the indented precipitate.

The diffraction pattern shown in Fig. 5 obtained for AM50 based specimens with increasing Zn content confirm the presence of ß- and τ-phase. The concentration of other precipitates is obviously too low to give suitable diffraction pattern. However the results are consistent with the microstructural study above, showing that a certain amount of Zn is required to reduce the ß phase fraction remarkably. Even though the amount of τ-phase is increasing a clearly reduced intensity of the ß-phase is only visible if the Zn content has reached 3 wt%. Furthermore the clearly visible shift of the highest intensity ß-phase peak indicates that there is an incorporation of Zn into the ß-phase contracting the lattice, which is consistent with the EDX results. Experimental evidence for the existence of two types of τ-phases is found in the diffraction pattern as well (Fig. 5), with the only copper containing alloy AZC501 showing the same diffraction peaks associated with τ-phase as the zinc containing alloys AZC5x1 ($1 < x < 4$). This suggests that Cu can replace Zn in the τ-phase forming $Mg_{32}(Al,Cu)_{49}$ if there is no or not enough Zn available. However it should be noted that the amount of τ-phase in the alloy AZC501 is rather low and thus the intensity of the possible peaks is weak making a trusted identification difficult. Furthermore there is one peak at 41° which can not be assigned to any known phase.

For increasing the tolerance limit it is important that the impurities are incorporated or embedded in electro-chemically more compatible precipitates with the matrix. Elemental mapping was performed on a selected region of the alloy AZC531 to demonstrate the distribution of various alloying elements and impurities in the

different phases (Fig. 6). Three intermetallic phases are visible in the selected region including Al_8Mn_5, ß- and τ-phase. The ß-phase in this alloy is composed from Mg, Al and Zn, but there are no detectable levels of impurities (Cu and Fe) present. This is different for the τ-phase, which is clearly composed from Mg, Al, Zn and Cu, suggesting that this phase is well suited for incorporation of Cu. Additionally a slight enrichment of iron in the τ-phase is detected, but it is much less compared with the level in the AlMn-phases. The third phase Al_8Mn_5 is not only build-up by Al and Mn, but contained a remarkable amount of Fe as well.

5.4 Mechanical properties

The main intention here is not to give detailed information about the mechanical properties, but to demonstrate simply that the new alloy has a comparable ductility to the standard alloy AM50. For this purpose the stress-strain curves of the two mostly used magnesium alloys AM50 and AZ91 are compared with the recently developed secondary alloy AZC1231 and the new AZC531 (Fig. 7). Latter alloy has the best strength values with sufficiently high ductility close to the value of AM50. The elongation to fracture is about 10% for the recycling and 12% for the standard AM50 alloy. Thus it can be stated that the ductility requirement for the new alloy is fulfilled. Please note that all specimens were tooled from gravity cast material, thus the values might be lower than expected from high pressure die cast or even extruded material.

5.5 Corrosion

5.5.1 Effect of Zn on the passive film formation

The visual impression, based on the colour of corroded specimens with or without Zn after immersion in de-ionized water, appears to be different, but a more detailed look on the surface with higher magnification shows a similar morphology (Fig. 8). There are hydroxide needles on the top surface and underneath a dense layer structure becomes visible. The only difference is the number of cracks in the layer being higher for the AM50 compared with AZ53 or AZC531. In order to monitor and to better understand the passive film formation on the three alloys, the surface films were studied by XPS analysis. Figure 9 shows the concentration of oxygen (O 1s) for the 3 alloys after 1 and 24 hours of immersion in the deionised water. After one hour no significant difference was observed for the different alloys, indicating that the starting mechanism is more or less the same. However, after one day of immersion an influence of Zn on the film formation becomes visible. The film formation on the

surface of AZ specimens has slowed down indicated by a reduced thickness of the oxygen depth profile. This is also consistent with the observed reduced susceptibility against cracking which can be expected for the thinner AZ films (Fig.8).
Using region scans offers the possibility to study the chemical composition during film growth. As one can see in figure 10, the composition of the surface of the three alloy systems differs more if the exposure time in the corrosive environment is increasing. Corrosion obviously starts in all three alloys with hydroxide formation (1 h immersion Fig. 10 a). After 24 hours AM50 shows directly on the surface a stronger hydroxide formation also verified by the $Mg(OH)_2$ signal measured after sputtering (increase of thickness). In deeper regions magnesium oxide was detected as well. In comparison, the two AZ systems reveal a relatively strong decrease of $Mg(OH)_2$ formation, which may indicate a better corrosion performance. Less magnesium dissolves and as a consequence less $Mg(OH)_2$ can grow on the surface and the film thickness was reduced. It is most likely that the noticed reduction of hydrogen evolution on τ-phase compared with ß-phase is responsible for the slowed down dissolution of Mg in the two AZ systems. However, $Mg(OH)_2$-MgO formation was still observed but on a much lower level. The influence of Cu in the AZC alloy can be seen in a slightly enhanced oxide formation compared with the pure AZ, but it is still less than in the AM50 alloy. The magnesium corrosion products detected, $Mg(OH)_2$ closer to the surface and MgO closer to the bulk are in good agreement with findings of other XPS studies on corroded magnesium [30-32].
Finally the binding conditions of the alloying elements aluminium, zinc and copper in the film on the AZC531 alloy were studied to check whether they are contributing to a mixed oxide film or not. In Figure 11 the results are presented in the form of elemental depth profiles. It is obvious that zinc and copper are only present in the bulk metallic state throughout the whole thickness of the layer without any kind of oxide formation. Only Al shows a weak formation of Al_2O_3 close to the surface. Due to the physical effects (plasmons) during the XPS measurements peak broadening occurs, but without any influence for the evaluation of the data. Thus only Al contributes to the passive/oxide film formation.

The interesting role of Zn was studied in more details using EIS measurements of AM50 based alloys with increasing Zn content immersed for 24 hours in 5% aqueous NaCl solution. The evaluation of the Nyquist plots indicated that all specimens suffer from active corrosion after 24 hours immersion into the 5% NaCl solution. An

inductive loop at low frequencies suggests that localised corrosion occurs. The charge transfer resistances as a function of increasing Zn content for alloys with either 40 ppm Ni or 0.5 wt% Cu are displayed in Fig. 12. It is clearly visible that the resistance of the specimens against dissolution is increasing in the presence of copper if the Zn content is increasing (Fig. 12b), correlating with the content of τ-phase in the alloy. In the presence of Ni this effect is not clearly visible (Fig. 12a). This suggests that the negative effect of nickel is not really neutralised by the formation of τ-phase. In contrast at low Zn contents the stability of the surface is reduced and alloying with more than 2 wt% of Zn is required to reach a level comparable to the alloy without Zn (AM50). However the more critical impurity levels of iron and nickel in latter alloy (see Tab. 1, specimen 70) are the lowest in the whole series, thus this may have an additional contribution to the relatively high charge transfer resistance measured for this specimen.

5.5.2 Effect of Zn on the general corrosion resistance

With the aim to understand the correlation of microstructure and corrosion resistance as a base for further optimisation of the alloy composition the influence of Zn on the corrosion resistance was determined. The corrosion results of immersion tests in 3.5% NaCl are shown in Fig. 13. The effect of Zn addition is noticeable in the presence of both impurities. For Ni (Fig. 13 a) the corrosion rate is gradually decreasing from about 23 to 8 mm/year if the Zn content is increased from 0 to about 4.3 wt%. The effect is not that large because the addition of Zn does not result in the formation of special phases which are able to incorporate Ni to a larger amount.

However the τ-phase was actually selected due to the fact that it can incorporate large amounts of Cu while being more compatible to the matrix than the ß-phase. Therefore, it is no surprise that the increase of the Zn content and thus the fraction, percentage increase of the τ-phase in combination with the reduction of other more detrimental phases is much more effective in increasing the corrosion resistance in the presence of Cu impurities compared with Ni (Fig. 13 b). The increasing Zn content from 0.02 wt% to 4.16 wt% reduces the corrosion rate from 33 to only 1 mm/year. Such a low value is comparable to the performance of high purity alloys in spite of the fact that this alloy contains 0.5 wt% Cu.

Additionally, salt spray tests were successfully performed to validate the immersion results. The corrosion rates as a function of Zn content are displayed in Fig. 14 a for alloys with a constant Ni impurity level of approximately 0.004 wt% (40 ppm) and in Fig. 14 b for alloys with a constant copper impurity level of 0.5 wt%. It is obvious, that the trend in both corrosion tests is the same, indicating that an increasing Zn content of up to 4 wt% is beneficial for the corrosion resistance of an Mg/Al alloy that contains 5 wt% of Al. Differences in the actual corrosion rates of both tests can be explained by the different conditions of the corrosive environment. In the immersion test the specimens are completely immersed in a large volume of solution with constant pH, while in the salt spray test the specimen is continuously covered by a thin film of solution, which should result in earlier saturation of the solution film with corrosion products and thus an earlier and denser formation of a passive film on the surface. This is consistent with the much lower corrosion rates observed under salt spray conditions. Furthermore the sampling period of both tests is extremely different (400 hours in immersion and only 48 hours in salt spray) and corrosion rates may change with exposure time.

Considering the Ni and Cu results the largest improvements in corrosion resistance are obtained by Zn additions between 0 and 2 wt%. A further increase of the Zn content reveals only minor improvements of the corrosion resistance thus the content of Zn should be around 2 wt% to guarantee reasonable good corrosion rates at an impurity level of either 0.004 wt% Ni or 0.5 wt% Cu. However in a recycling alloy fluctuations of impurity contents can be expected thus an alloy with about 3 wt% Zn is suggested to tolerate such fluctuations as well as being able to deal with a combination of increased and/or fluctuating impurities levels of Ni, Cu and Fe. Nevertheless, the corrosion rates for the alloy with 3 wt% Zn contaminated with Ni showing about 3 mm/year in salt spray and about 10 mm/year in immersion condition already imply that the selected impurity level of 40 ppm is too high. Thus the final step would be to determine the tolerance limits of the selected alloy with 5 wt% Al and 3 wt% Zn.

5.5.3 Effect of impurities on the corrosion resistance (tolerance limits for the alloy AZ53)

The amount of impurities which can be incorporated without exceeding the tolerance limit is visible in Fig. 15. The figure shows the influence of increasing Ni and Cu contents on the corrosions rate of the alloy AZ53 determined by immersion and salt

spray test. The triangle in the figures represents the corrosion performance of the high purity AM50 in the respective corrosion test. The tolerance limit is given when the corrosions rate of the secondary alloy AZ53 equals or slightly exceeds the corrosion rate of the standard alloy AM50. The resulting tolerance limits are summarized in Table 5. It is interesting to note that both corrosion tests reveal similar and comparable values, in spite of having different corrosion rates, suggesting that both tests are suitable to determine tolerance limits. Obviously, the sensitivity against impurities or the effect of the impurities on the corrosion mechanism is similar under the two test conditions. However the results clearly suggest that the modification of the composition by adding 3 wt% Zn and thus of the microstructure was successful in increasing the tolerance limits especially for copper. The new alloy can now tolerate up to 0.7 wt% Cu instead of the 0.01 wt% of the AM50A as suggested by the ASTM B94-07 standard. However the effect of the microstructural changes on the possible nickel up-take is limited and the maximum content of 20 ppm taken from the experimental data is the same as the maximum allowance in the ASTM B94 -07 standard for AM50A. However, the tested high purity AM50 alloy used for determining the tolerance limit of the AZ53 alloy had very low impurity content (2 ppm Ni, 7 ppm Fe and 77 ppm Cu) and thus a much better corrosion resistance with a lower corrosion rate as one would expect for the AM50 alloy with 20 ppm Ni. This implies that the microstructural changes introduced were also effective in improving the tolerance limit for Ni, even though not that successful as for Cu, but still as good as an AM50A with only 2 ppm Ni. Another interesting aspect visible in the diagrams of Fig. 15 is the existence of more or less two different slopes, indicating two concentration ranges with different effect on the corrosion rate. At low impurity levels the increase of the corrosion rate with increasing impurity concentration is lower compared with increases at higher impurity levels. For Cu this behaviour is quite evident while a similar effect for Ni is not that clear. Correlations with the microstructure gave evidence that this is related to the existence of critical intermetallics. At low Cu contents more or less all copper is incorporated into the τ-phase with only minor effects on the corrosion resistance. However if the amount of copper exceeds a certain limit given by the saturation of the τ-phase (not necessarily identical with the tolerance limit) more critical phases such as Q-phase and binary MgCu-phases form, causing the observed change in the slope. For Ni the uptake of the τ-phase is very limited (if at all) and a change occurs already at a few ppm Ni.

6 Discussion

The present paper deals with a correlation of thermodynamic modelling, microstructural studies and corrosion behaviour of a class of secondary magnesium alloys. The main aim is to demonstrate and evaluate a new approach of embedding and neutralisation of impurities in the microstructure offering new design possibilities for corrosion resistant magnesium alloys having higher tolerance limits against impurities. This concept has produced so far two different approaches. The first approach was realised mainly by increasing the amount of ß-phase, thus improving the ß-phase network and the corrosion barrier function of it. The τ-phase was already used in this approach to incorporate the Cu impurities and to contribute to the network formation, but played only a minor role altogether. The outcome was a more impurity tolerant alloy AZC1231, but due to the high volume of intermetallics in the microstructure the ductility was very limited [11, 14]. The second approach described in the present paper focussed on the τ-phase. This was necessary because it was decided to develop a new more ductile secondary alloy. Therefore the Al content had to be reduced. As a consequence the amount of ß-phase is decreasing loosing its ability to form a dense network providing the barrier function. At this point two findings were important. Firstly the τ-phase was identified to be electrochemically more compatible to the magnesium matrix than the ß-phase and secondly the negative effect of Zn additions on the ductility of an AM50 based alloy is much lower than for the same amount of Al addition. These findings lead to the idea to add Zn to the AM50 alloy and try to replace the ß-phase by the τ-phase. The thermodynamic modelling using the Calphad concept was successfully used to verify this idea and to estimate the required Zn additions as well as understanding the solidification of these alloys. The Zn influence on the phases present and their phase fraction in the respective alloy was a usefully information to optimise the alloy composition. The selected Zn concentration of 3 wt% is a compromise between sufficient suppression of the ß-phase, preventing formation of new Zn-rich phases, ductility and cost requirements. It appears likely that the ß-phase formation might be completely suppressed if the Zn content is further increased but that would be on cost of formation of additional phases, ductility and cost of the alloy.

The final castings revealed reasonable agreement between the predictions of the model and the real microstructures indicating that the modelling is a suitable tool to

reduce the experimental effort in alloy design. However there are some deviations at lower Zn contents. The observation of the real microstructures and the XRD results indicate that the suppression of the ß-phase formation is not that much as predicted from the modelling. However if sufficiently Zn is present the prediction appears to be in a much better agreement e.g. for the selected secondary alloy composition AZC531. With increasing Zn content the difference between the starting temperatures of τ-phase and ß-phase solidification (formation) is increasing, thus there is already Al consumed before the formation of ß-phase would start, resulting in a reduced phase fraction. Thus, the existence of the τ-phase and the possibility to suppress ß-phase formation for AZ type of alloys with increasing Zn contents ($C_{Al}>C_{Zn}$) is evident from both modelling and experiments.

Surprisingly there is not much information about the τ-phase and its existence in magnesium alloys. The only reports are from ZA alloy systems were the content of Zn is higher than the content of Al [33-36] and one for GTA welded AZ31B where the τ-phase was identified in the weld metal [37]. To the knowledge of the authors there are no other reports for AZ systems confirming the presence of τ-phase even if they have a similar composition than the secondary alloy e.g. AZ63. None of the early and of the recent publications are confirming the existence of the τ-phase in AZ63 [38-41]. The missing identification of τ-phase pointed to the important role of Cu in the alloy. All the modelling and the experimental determination of the microstructure in the present study were performed in the presence of 0.5wt% Cu, which is in contrast to the published work mentioned above. Indeed Scheil calculation for the alloy AZ53 (not shown in the present paper) revealed that not only the amount of τ-phase is reduced, but also the starting temperature of solidification is shifted from 392 (AZC531) to 339°C (AZ53). This implies that the smaller amount can be easily hidden in the eutectic seam between the grain boundaries and/or that the formation is suppressed because the solidification of the remaining melts is too quick in this temperature range. The conclusion is that not only Zn is responsible for the formation of the τ-phase, but it is the Cu impurity content that stabilizes τ and promotes the formation. This is an interesting mechanism for secondary alloys as basically the Cu impurities stimulate the formation of the phase which contributes to the neutralisation of detrimental Cu effects on the corrosion resistance.

This is important because for Cu and Ni the possibilities to remove them from the melt are limited and/or too expensive, thus the aim of the present alloy development was to leave as much as possible Cu and Ni impurities in the alloy while still providing a corrosion resistance similar to the high purity AM50. As already discussed iron impurities can be quite easily removed or controlled by melt treatment with manganese or manganese chloride [31], thus they are no concern. From the elemental mapping it is obvious that the τ-phase is well suited for incorporation of Cu. In the ternary Mg-Al-Zn system the phase ($Mg_{32}(Zn,Al)_{49}$) and in the Mg-Al-Cu system the phase ($(Al_xCu_{1-x})_{49}Mg_{32}$) exist, both with same structure and nearly the same lattice parameters, which suggests that Zn and Cu are interchangeable in the τ-phase ($Mg_{32}(Zn,Al,Cu)_{49}$) [42-44]. Thereby the copper content in the τ-phase remain on a much lower level compared with other Cu containing phases in the Mg-Al-Zn-Cu system (e.g. $MgCu_2$, Mg_2Cu, $Al_7Cu_3Mg_6$), suggesting that the τ-phase is less detrimental in the magnesium matrix from the electro-chemical point of view. All those features of the τ-phase are very important for the uptake of fluctuating copper levels which can appear in secondary alloys produced from post-consumer scrap. Unfortunately there is no similar behaviour observed for Ni. The only active mechanism might be the embedding of Ni and Ni-rich intermetallics in the τ- and ß-phase thus separating them from direct contact with the matrix. However, sometimes a slight enrichment of iron and nickel can be noticed in the τ-phase according to the mapping results, thus it may contribute as well in increasing their tolerance limits by embedding iron and nickel remains that are not incorporated by Al_8Mn_5. This finding has to be verified as most of the EDX point analysis has not shown larger enrichment of iron and especially of nickel in the τ-phase. Sometimes some iron was detected, but for nickel no real evidence was seen so far that major fractions are incorporated into the τ-phase. However it should be noted that the Ni contents with a maximum of about 40 ppm are too low for identifying Ni intermetallics or pure Ni in the matrix. So far nickel is only detected when it is enriched in Al_8Mn_5 intermetallics together with Fe. Thus the above statement about embedding is rather speculative and no real experimental evidence was found so far. As a consequence the nickel tolerance limit of the recycling alloy should be still comparably low to guarantee sufficient corrosion resistance.

The newly developed secondary alloy AZC531 has revealed a similar corrosion resistance (immersion, salt spray) compared with the conventional high purity alloy AM50 in spite of the incorporation of higher impurity levels especially copper. This surprising result is mainly based on the unique electro-chemical properties of the τ-phase compared with the ß-phase. The τ-phase is not only less detrimental in the magnesium matrix but is also able to incorporate much higher Cu concentrations compared with the ß-phase, preventing the formation of additional Cu-rich phases. While the electro-chemical properties of the ß-phase as well as the influence of the ß-phase distribution in the magnesium matrix were sufficiently characterised and very well understood over the past years [15-25, 28, 29], there is only limited information available about the properties of the τ-phase [37]. Summarising the references, the ß-phase is cathodic to the matrix (E_{Corr} between -1.2 and -1.3 V_{SCE}) and therefore the single localised ß-phase precipitates in the AM50 type of alloys are active galvanic couples and places for discharging hydrogen ions which is an important step in the corrosion process of Mg alloys. It is also established that the ß-phase is able to incorporate Zinc [11, 16, 19]. The reports of the effect of Zn incorporation on the electro-chemical properties of ß-phase are not consistent in the literature and may also depend on how much Zn is in the ß-phase. For example, Lee et al. [19] are reporting a negative shift of the corrosion potential, while Lunder et al. [20] are finding no shift at all and Mathieu et al. [16] a positive shift. The latter result is in good agreement with the present findings for the two ß-phases in the study. However phases with higher zinc contents were only studied by Lee et al., but they have not the composition of the τ-phase and are most likely related to ß-phase. The τ-phase (with a composition of 39 at% Mg, 42 at% Zn and 19 at% Al) is reported to be cathodic to the Mg matrix and the Volta potential difference relative to the Mg matrix of the τ-phase is larger compared with Al_8Mn_5-phase [37]. However, the τ-phase has a large solubility range for the noble alloying elements Cu and Zn, thus larger variations are expected in the electrochemical properties related to the various compositions possible. Therefore two quite different τ-phases were selected in the present study. A pure one containing 60 wt% Zn, 17 wt% Al and 23 wt% Mg and a second one with joint solid solution of Zn and Cu having a composition of 31 wt% Zn, 32 wt% Al, 9 wt% Cu and 28 wt% Mg. The latter one is closer to real compositions of τ-phases in the microstructure of the AZC alloys, while the first one is close to the composition given by Ben-Hamu et al. [37]. Most likely due to the high zinc content

the corrosion potential of the pure τ-phase is the most noble from the four intermetallics reaching a value of around -1050 $mV_{Ag/AgCl}$. The solid solution Cu rich τ(Cu)-phase is, in spite of the copper addition, less noble which can only be related to the reduced Zn content. However with around -1150 $mV_{Ag/AgCl}$ this τ(Cu)-phase is still more noble than the ß(Zn)-phase (-1250 $mV_{Ag/AgCl}$) and the pure ß-phase (-1275 $mV_{Ag/AgCl}$). Considering the fact that the free corrosion potential of ß-phase is reported to be similar to Al_8Mn_5-phase [16], the present results of the corrosion potentials are in agreement to the findings of Ben-Hamu at al. [37].

This would normally imply that the most noble phase would be the most detrimental regarding the galvanic coupling with the matrix. However this is only partly true if the two ß-phases are compared. Here the addition of Zn is shifting the potential to more noble values and as a consequence the galvanic current in a coupling between ß and matrix is also increasing. This observation is consistent with the findings reported in literature [16, 20]. However for the τ-phases this is not true anymore. Interestingly, there is a much larger potential difference between τ- and τ(Cu)-phase as a driving force compared with the potential difference between ß- and ß(Zn), but there is almost no difference in the galvanic current of the two τ phases in a coupling with the Mg matrix. Furthermore the galvanic current of τ-phase in the coupling with Mg matrix is by far lower compared with a coupling of ß-phase and matrix. The only possible explanation for this behaviour is the much higher overvoltage for hydrogen formation of the τ-phases in comparison with the ß-phases, which is also evidence in the polarisation curves of the intermetallic phases. Zinc appears to be a very interesting alloying element for improving corrosion resistance of Mg alloys by forming intermetallics with high compatibility to the matrix. As anodic and cathodic processes are normally interlinked a reduced cathodic hydrogen formation suppresses the anodic dissolution of the magnesium as well. Hydrogen ion discharging on the cathodic regions is an essential mechanism in the corrosion of Mg, consuming the electrons left over by the dissolution of the Mg in the anodic regions. If discharging is suppressed the dissolution is suppressed as well. It is known that Zn has a high over-potential for hydrogen generation [45]. This suggests that a certain amount of Zn is required to transfer this behaviour to other metallic/intermetallic phases. The 5 wt% Zn in the ß-phase is not sufficient while the 30wt% in the τ-phase seems to be enough to hinder the hydrogen discharging at the τ-phase. This is consistent with an

observation in the MgZnCa system that an increase of the zinc content to 30 wt% resulted in an alloy with a very low level of hydrogen formation [46]. It would be interesting to study these effects in more details and to prove that zinc has this effect in other magnesium intermetallics or alloys as well. In the AZC system the amount of the ε-phase (MgZn) and the Φ-phase ($Mg_5Zn_2Al_2$) is increasing with increasing zinc content. In both phases the Zn content is above the 30 wt% limit, thus they are ideal candidates for proving the idea of the overvoltage transfer and for further optimising the corrosion performance of AZC based secondary alloys.

There is opposed information available in literature according to the effect of increasing solid solution aluminium contents of the matrix on the galvanic current in coupling with ß-phase. Some papers do report an increase in the galvanic current [19, 20, 29] and others [16] a decrease compared with pure Mg. However this might be an effect of different purity of the pure Mg. In the same way an increasing Al content is sometimes reported to be beneficial in reducing the galvanic current density and sometimes not. Consistency is found in the observation that there is a limit between 6 and 9 wt% Al, above which negative effects on the current density were found. In our study we remained underneath those values and thus we can only report of a positive effect of increasing solid solution Al contents on reducing the galvanic current density. Our results are in good agreement with the finding from Mathieu et al. [16]. Increasing general corrosion resistance with increasing Al alloy content caused by Al enriched superficial layers is a possible explanation for the reduced galvanic current in the couple with either ß- or τ-phase.

The formation of superficial layers is another important factor influencing the corrosion resistance of magnesium alloys. A dense and uniform layer can greatly reduce the corrosion rate. The XPS studies on the superficial layers formed on the surface of an AZC531 alloy indicate that mainly MgO and $Mg(OH)_2$ is present in the layers. From the three main alloying elements Al, Zn and Cu only Al is found in an oxidised state thus contributing to the superficial oxide/hydroxide film. Zinc and Cu are only detected in the metallic state. As they are not forming oxides or hydroxides they should have no direct influence on the performance of the superficial film. This implies that Zn and Cu are more likely contributing to the stability of the surface layers by preventing or at least reducing the formation of detrimental galvanic cells on the surface. Different elemental composition of the particles and the high

corrosion current density close to the galvanic active phases (particles) are disturbing and/or preventing the formation of dense uniform superficial films. This is consistent with observation made during and after the corrosion tests. For Zn-free alloys a more localised deep pitting type of attack is observed, while in the presence of 3 wt% zinc the corrosion mechanism is shifting to a more uniform general attack in combination with shallow filiform type of corrosion morphology. Even though Zn is not directly involved in the superficial film formation, it may contribute to a denser $MgO/Mg(OH)_2$-film growth by reducing the influence of detrimental galvanic cells on the film formation and uniformity. Furthermore, there seems to be a reduced oxide film thickness in Zn containing alloys, which is possibly related to the τ-phase and its influence on the kinetics of the corrosion process by suppressing hydrogen formation at the cathodic τ-phase.

However as discussed above the ß-phase can be detrimental for the matrix if it is present in single localised precipitates and can not form a dense corrosion barrier. In that case it would be much better to completely remove the ß-phase and replace it by a less detrimental phase such as the τ-phase. This was only partly possible by adding Zn to a Cu contaminated AM50 alloy. In the studied range no complete suppression of ß-phase formation was achieved. Nevertheless the additional benefit for recycling alloys is the fact that the τ-phase is capable to incorporate a large amount of Cu impurities, without too much negative effects on the corrosion performance, but unfortunately for Ni such a phase is not available at the moment. Anyway, the concept was quite successful in designing a more impurity tolerant alloy based on the AM/AZ system [47]. Compared with the ASTM standard the tolerable copper content is largely extended reaching 0.6-0.7 wt% and also the tolerable nickel content is improved, but still has to be kept lower than 20 ppm (0,002 wt%) if the salt spray corrosion rate should not exceed 1 mm/year which is an acceptable corrosion rate for magnesium alloys under salt spray conditions. The salt spray and immersion tests have demonstrated that under these conditions the secondary alloys within the above tolerance limits are performing better or similar to the high purity standard alloy AM50. Outdoor exposure tests are currently running for the AZC531/AM50 alloys and from the experience with the alloys AZC1231/AZ91 one may expect a poorer performance of the secondary alloy compared with the standard alloy [48]. The main difference was in the superficial layer formation, which was much faster for the secondary alloy leading to accelerated material loss as the layer started to flake

off in dry periods. This was not observed for the pure standard alloy. However it should be noted that the performance of the secondary alloy was still much superior in comparison with a standard alloy having the same impurity level.

Nevertheless the achieved improved tolerance limits are important for secondary alloys which have difficulties in reaching the high purity requirements of primary magnesium for providing good corrosion resistance if post-consumer scrap is used for recycling. Cu and Ni are normally not removed and the limits are only reached by blending with high purity primary material, which is not the best solution if the scrap contains larger amounts of impurities. That is actually the main reason why magnesium based post consumer scrap is still not used as a source for secondary alloy production. This problem is approached now and partly solved by the new secondary alloy AZC531 with the improved tolerance limits, but some major open questions are still remaining:

1) What happens with the microstructure if the Al content must be further lowered e.g. for rolling applications. However the answer requires more studies which are not part of the present investigations. Nevertheless, one can assume that reasonable corrosion resistance is obtained if sufficiently ß-phase is converted into τ-phase. Correlating the phase fractions obtained from modelling, the real composition, microstructure and corrosion performance results for specimens with an constant Al content of 5 wt% suggests that this appears to be the case if the Al/Zn ratio is in the range between 2 and 1, thus between MgAl5Zn5Cu1 (AZC551) and MgAl5Zn2.5Cu1 (AZC531). Further fine-tuning might be required with changing Al and Zn contents.

2) How is the workability of the alloy under industrial conditions? Processing trials were so far performed only on laboratory scale for gravity casting, high pressure die casting, semi-solid processing and extrusion indicating no problems and a similar behaviour compared with AM50. However, based on the known performance of AM50 no major problems are expected if the new alloy is processed by commercial processes such as high pressure die casting on the one hand and extrusion or forging on the other hand.

3) What are the effects of changing composition and processing on the microstructure and how are these changes interlinked with corrosion and mechanical properties? It is obvious that there are various influences like size and distribution of

the precipitates, grain size, work hardening effects etc. but generally it can be expected that for every property requirement a suitable alloy is available as the AZC system covers a whole group of alloys arranging from AZC1231 over AZC531 down to AZC211 or similar alloys.

From the processing point of view it should be possible now to recycle magnesium post-consumer scrap and magnesium alloys contaminated with copper and/or nickel by simple re-melting having reduced negative effects on the corrosion resistance. While the alloy AZC1231 is a suitable secondary alloy for AZ91 type of scrap the new alloy AZC531 is supposed for AM50 type of scrap and there is potential to extent the same concept to an alloy AZC321 or AZC211 offering a secondary alloy for AZ31 based scrap. The introduction and existence of three secondary alloy classes offers the chance that almost all commercial alloys can be recycled without using too much primary magnesium alloys or alloying elements for alloying or diluting the scrap melt. Due to the three secondary alloy classes the alloy adjustment is reduced to minimum saving primary magnesium or other alloying elements with a positive effect on the lifetime assessment. Therefore, it can be concluded that with this new alloy classes the gap in the recycling of magnesium alloys can be further closed maybe generating a positive effect on the general use of magnesium as well.

7 Conclusions

1) Magnesium alloy design considering the influence of the alloying elements on the formation of intermetallic phases in the alloy, their electro-chemical properties and the ability to incorporate impurities can be an alternative to the standard high purity concept to guarantee a good corrosion resistance of magnesium alloys.

2) Zinc addition to a copper containing AM50 alloy promotes the formation of τ-phase ($Mg_{32}(Zn,Al,Cu)_{49}$) and suppresses the formation of ß-phase ($Mg_{17}Al_{12}$).

3) In spite of having a higher potential difference, the τ-phase is less detrimental in a galvanic coupling with a magnesium matrix compared with the ß-phase. This is explained by higher hydrogen over-potential of the τ-phase due to the high zinc content. The over-potential is effectively hindering the discharge of hydrogen ions at the cathodic sides and thus the whole magnesium corrosion process.

4) The τ-phase has a large solubility range for copper, thus replacing ß- by τ-phase is suitable to increase the tolerance limit for copper in AZ based magnesium alloys.

5) The AZC alloy system with an aluminium content of less than 5 wt% and an Al/Zn ratio between 2 and 1 seems to offer interesting alloy alternatives for producing ductile secondary alloys with increased tolerance limits.

8 Acknowledgements

The development of the new corrosion resistant magnesium secondary alloy is a joint project of the Institut für Metallurgie of the Technische Universität Clausthal and the GKSS Forschungszentrum Geesthacht GmbH and is supported by the Deutsche Forschungsgemeinschaft within the Schwerpunktprogramm 1168 “InnoMagTec” Project-Nr. DI492/9-3, KA 1053/9-3. The authors acknowlegde the financial support of the Deutsche Forschungsgemeinschaft.

9 References

[1] A. Ditze, C. Scharf, ERZMETALL, 57 (2004) 251-257.

[2] D. Albright, J. Haagensen, Life cycle inventory of magnesium, in: 54th Annual World Magnesium Conference: Magnesium Trends, International Magnesium Association, Toronto, Canada, 1997, pp. 32-37.

[3] S. Ehrenberger, S. Schmid, H. Friedrich, Magnesium production and automotive applications: Life-cycle analysis focussing on greenhouse gases, in: 16th Magnesium Automotive and User Seminar, Aalen, Germany, 2008.

[4] P. Koltun, A. Tharumarajah, S. Ramakrishnan, Life cycle environmental impact of magnesium automotive components, in: Magnesium Technology 2005, 2005, pp. 43-48.

[5] A. Pedersen, A. Fischersworring-Bunk, M. Kunst, I. Bertilsson, I. de Lima, M. Smith, M. Wappelhorst, P. Bakke, S. Sereni, M. Durando, Light weight engine construction through ectended and sustainable use of Mg-alloys, SAE paper 2006-01-0068, 2006.

[6] S. Ramakrishnan, P. Koltun, Resources Conservation and Recycling, 42 (2004) 49-64.

[7] A. Ditze, C. Scharf, Recycling of Magnesium, Papierflieger Verlag, Clausthal-Zellerfeld, Germany, 2008.

[8] A. Ditze, C. Scharf, C. Blawert, K.U. Kainer, G.E.D. Morales, Magnesiumsekundärlegierung, DE 10 2005 033835 A1, 2005

[9] A. Ditze, C. Scharf, C. Blawert, K.U. Kainer, G.E.D. Morales, Magnesium Alloy, WO 2007/009435 A1, 2007

[10] C. Scharf, A. Ditze, A. Shkurankov, E. Morales, C. Blawert, W. Dietzel, K.U. Kainer, Advanced Engineering Materials, 7 (2005) 1134-1142.

[11] C. Blawert, E. Morales, K.U. Kainer, C. Scharf, P. Živanović, A. Ditze, Development of a new AZ based secondary magnesium alloy, in: 65th Annual World Magnesium Conference, Warsaw, Poland, 2008, pp. 57-64.

[12] C. Blawert, E. Morales, W. Dietzel, N. Hort, K.U. Kainer, C. Scharf, A. Ditze, F. Endres, Corrosion properties of secondary AZ91 alloys, in: Magnesium Technology 2005, 2005, pp. 447-450.

[13] C. Blawert, E. Morales, W. Dietzel, K. Kainer, C. Scharf, A. Ditze, Influence of the Copper Content on Microstructure and Corrosion Resistance of AZ91 Based Secondary Magnesium Alloys, SAE paper 2006-2001-0254, 2006.

[14] C. Scharf, P. Zivanovic, A. Ditze, K. Horny, G. Franke, C. Blawert, K. Kainer, E. Morales, Giesserei, 94 (2007) 38-50.

[15] F. Andreatta, I. Apachitei, A.A. Kodentsov, J. Dzwonczyk, J. Duszczyk, Electrochimica Acta, 51 (2006) 3551-3557.

[16] S. Mathieu, C. Rapin, J. Steinmetz, P. Steinmetz, Corrosion Science, 45 (2003) 2741-2755.

[17] G.L. Song, A. Atrens, Advanced Engineering Materials, 1 (1999) 11-33.

[18] R. Ambat, N.N. Aung, W. Zhou, Corrosion Science, 42 (2000) 1433-1455.

[19] C.D. Lee, C.S. Kang, K.S. Shin, Metals and Materials-Korea, 6 (2000) 351-358.

[20] O. Lunder, J.E. Lein, T.K. Aune, K. Nisancioglu, Corrosion, 45 (1989) 741-748.

[21] K. Nisancioglu, O. Lunder, T.K. Aune, Corrosion Mechanism of AZ91 Magnesium Alloy, in: 47th Annual World Magnesium Conference: Past to Future, IMA, Cannes, France, 1990, pp. 43-50.

[22] G.L. Song, A. Atrens, M. Dargusch, Corrosion Science, 41 (1999) 249-273.

[23] M.D. Bharadwaj, S.M. Tiwari, Y.M. Wang, V. Mani, Micro galvanic corrosion behavior of Mg alloys as a function of aluminum content, in: Magnesium Technology 2008, 2008, pp. 389-391.

[24] S. Maddela, Y.M. Wang, A.K. Sachdev, R. Balasubramaniam, The Influence of Beta ($Mg_{17}Al_{12}$) Phase Distribution on Corrosion Behavior of AM50 Alloy in NaCl Solution, in: Magnesium Technology 2009, 2009, pp. 321-331.

[25] S. Sundarraj, M.D. Bharadwaj, S.M. Tiwari, Effect of composition and cooling rate on the beta phase formation in Mg-Al alloy, in: Magnesium Technology 2008, 2008, pp. 329-330.

[26] S.L. Chen, S. Daniel, F. Zhang, Y.A. Chang, X.Y. Yan, F.Y. Xie, R. Schmid-Fetzer, W.A. Oates, Calphad-Computer Coupling of Phase Diagrams and Thermochemistry, 26 (2002) 175-188.

[27] J.D. Hanawalt, C.E. Nelson, J.A. Peloubet, Transactions of the American Institute of Mining and Metallurgical Engineers, 147 (1942) 273-298.

[28] C. Blawert, E. Morales, G. Wiese, V. Kree, W. Dietzel, S. Jin, E. Ghali, Correlations of microstructure and corrosion properties in HPDC AZ91, in: M.O. Pekguleryuz, L.W.F. Mackenzie (Eds.) Magnesium Technology in the Global Age, Conference of Metallurgists, COM 2006, Montreal (CDN), 01.-04.10.2006, 2006, pp. 295 - 314.

[29] C.D. Lee, C.S. Kang, K.S. Shin, Metals and Materials-Korea, 6 (2000) 441-448.

[30] S. Ardizzone, C.L. Bianchi, M. Fadoni, B. Vercelli, Applied Surface Science, 119 (1997) 253-259.

[31] M. Liu, S. Zanna, H. Ardelean, I. Frateur, P. Schmutz, G.L. Song, A. Atrens, P. Marcus, Light Metals Technology 2009, 618-619 (2009) 255-262

[32] M. Liu, S. Zanna, H. Ardelean, I. Frateur, P. Schmutz, G.L. Song, A. Atrens, P. Marcus, Corrosion Science, 51 (2009) 1115-1127.

[33] J. Zhang, Z.X. Guo, F. Pan, Z. Li, X. Luo, Materials Science and Engineering: A, 456 (2007) 43-51.

[34] J. Zhang, Z.-s. Li, Z.-x. Guo, F.-s. Pan, Transactions of Nonferrous Metals Society of China, 16 (2006) 452-458.

[35] Z. Zhang, R. Tremblay, D. Dube, Materials Science and Technology, 18 (2002) 433-437.

[36] Z. Zhang, R. Tremblay, D. Dubé, Materials Science and Engineering A, 385 (2004) 286-291.

[37] G. Ben-Hamu, D. Eliezer, C.E. Cross, T. Böllinghaus, Materials Science and Engineering: A, 452-453 (2007) 210-218.

[38] H. Altun, S. Sen, Materials & Design, 25 (2004) 637-643.

[39] M. Anik, I.M. Gunesdogdu, Materials & Design, 31 (2010) 3100-3105.

[40] C.L. Liu, Y.C. Xin, G.Y. Tang, P.K. Chu, Materials Science and Engineering a-Structural Materials Properties Microstructure and Processing, 456 (2007) 350-357.

[41] A. Beck, Magnesium und seine Legierungen, Julius Springer Verlag, Berlin, 1939.

[42] G. Bergman, J.L.T. Waugh, L. Pauling, Nature, 169 (1952) 1057-1058.

[43] F. Laves, K. Löhberg, H. Witte, Metallwirtschaft, -wissenschaft und -technik, 14 (1935) 793-794.

[44] G. Petzow, G. Effenberg, Ternary alloys, VCH Weinheim, 1993.

[45] W. Mannchen, A. Wibranetz, Elektrochemie, VEB Deutscher Verlag der Wissenschaften, Berlin, Germany, 1959.

[46] B. Zberg, P.J. Uggowitzer, J.F. Loffler, Nature Materials, 8 (2009) 887-891.

[47] C. Blawert, K.U. Kainer, W. Dietzel, A. Ditze, C. Scharf, P. Živanović, Duktile Magnesiumlegierung, DE 10 2008 020 523 A1, 2008

[48] C. Scharf, P. Zivanivic, A. Ditze, D. Fechner, C. Blawert, K.U. Kainer, Corrosion Resistant Magnesium Recycling Alloys, in: K.U. Kainer (Ed.) Magnesium : 8th International Conference on Magnesium Alloys and their Applications, Wiley-VCH, Weimar, Germany, 2009, pp. 1308-1315.

Table captions

Table 1: Composition of the alloys and intermetallic phases used for microstructural and corrosion studies (all data in wt%, Mg remain)

Table 2: Results of the galvanic coupling between Mg matrix with different Al content and the various intermetallic phases ß and τ a) average current density in $\mu A/cm^2$ b) mixed potential in $mV_{Ag/AgCl}$ after 20 h

Table 3: Phase fractions (%) for an alloy with 5 wt% Al, 0.5 wt% Mn, 0.5 wt% Cu and increasing Zn contents obtained from Scheil calculations

Table 4. Calculated composition variation of phases during Scheil solidification for a magnesium alloy Mg-5Al-0.5Mn-0.5Cu-3Zn (wt%), see Fig. 3. Composition ranges correspond to decreasing temperature during contact with liquid.

Table 5: Tolerance limits determined for the alloy AZ53 from immersion and salt spray corrosion tests based on the results presented in Fig. 15. The composition of the tested specimens is given in Tab. 1. The tolerance limits by definition are the maximum possible impurity contents of Cu or Ni in the alloy AZ53 which can be added without exceeding the corrosion rate of the high purity AM50 (reference) in the respective corrosion test.

Table 6: Comparison of intermetallic phases and intermetallic phase compositions in the real microstructure of AZC501 and AZC531alloys

Figure captions

Fig. 1: a) Polarisation curves of selected intermetallic phases in 5% NaCl solution (pH11), b) Estimation of the galvanic current in a possible coupling of ß and τ(Cu) with a magnesium matrix (HP-Mg), only schematic

Fig. 2: Current density measured during galvanic coupling between matrix and intermetallic phases in 5% NaCl solution, pH11 a) Coupling between pure magnesium and ß, ß(Zn) and τ(Cu), b) Coupling between Mg3Al and ß, ß(Zn) and τ(Cu) and c) Coupling of Mg6Al and ß, ß(Zn) and τ(Cu)

Fig. 3: Calculated phase fractions for a magnesium alloy with 5 wt% Al, 3 wt% Zn, 0.5 wt% Cu and 0.5 wt% Mn (Scheil model)

Fig. 4: SEM micrographs (BSE mode) showing the influence of Zn addition on the microstructure of AM50 based alloys a) AZC500 (AM50), b) AZC501, c) AZC511 and d) AZC531

Fig. 5: XRD diffraction pattern for various AM50 based alloys with increasing Zn content

Fig. 6: Microstructure and elemental mapping (EDX) of the elements Mg, Al, Zn, Cu, Fe and Mn revealing the distribution of each element in the different phases of an AZC531 alloy

Fig.7: Comparison of the stress-strain curves of the alloys AM50, AZ91, AZC1231 and the new alloy AZC531

Fig. 8: Comparison of the surface morphology of corroded specimens (immersion, 24 hours in de-ionised water) a) AM50 b) AZ53 and c) AZC531

Fig. 9: Oxygen depth profiles (XPS, O 1s) on AM50, AZ53 and AZC531 specimens after immersion of 1 and 24 hours in aerated de-ionized water (the lines are only guidance for the eye).

Fig. 10: XPS depth profile region scans (top=surface) of Mg 2p and detected binding states for the three alloys after a) 1hour and b) 24 hours immersion into de-ionized water

Fig. 11: XPS depth profile region scans (top=surface) of Al 2p, Zn 2p and Cu 2p (including all electron states 1/2 and 3/2) and detected binding states in the surface film of an AZC531 specimen after 24 hours immersion in de-ionized water

Fig. 12: Charge transfer resistance determined from EIS measurements performed on AM50 based specimens with increasing Zn content after 24 hours immersion in aqueous 5% NaCl solution a) alloys with 40 ppm Ni and b) alloys with 0.5 wt% Cu

Fig. 13: Corrosion rates for AM50 based alloys with increasing Zn content determined from hydrogen evolution measurements during long term immersion tests in aqueous 3.5% NaCl solution a) alloys with 40 ppm Ni and b) alloys with 0.5 wt% Cu

Fig. 14: Corrosion rates for AM50 based alloys with increasing Zn content determined from weight loss measurements after 48 hours salt spray testing using neutral 5% NaCl solution a) alloys with 40 ppm Ni and b) alloys with 0.5 wt% Cu

Fig. 15: Influence of impurities on the corrosion resistance of an AZ53 alloy. Tolerance limits defined by the performance of a comparable high purity AM50 alloy are marked by the dashed horizontal line. a) immersion test, 400 h, 3.5% NaCl, pH 6, nickel influence, b) immersion test, 400 h, 3.5% NaCl, pH 6, copper influence, c) salt spray test, 48 h, 5% NaCl, pH 6.5, nickel influence, salt spray test, 48 h, 5% NaCl, pH 6.5, copper influence

Table 1: Composition of the alloys and intermetallic phases used for microstructural and corrosion studies (all data in wt%, Mg balance).

specimen	Al [%]	Zn [%]	Cu [%]	Si [%]	Mn [%]	Fe [%]	Ni [%]
Zn influence on AM50 with 0.5 wt% Cu							
62 (AM50, reference)	4.9	0.02	0.0077	0.026	0.26	0.00068	< 2 ppm
63 (AZC501)	4.84	0.023	0.52	0.028	0.26	0.00092	< 2 ppm
133	5.4	0.49	0.49	0.026	0.27	0.00079	< 2 ppm
99	5	0.58	0.51	0.027	0.28	0.001	< 2 ppm
134 (AZC511)	5.43	1.02	0.5	0.027	0.26	0.0012	< 2 ppm
76	5.27	1.1	0.51	0.027	0.28	0.00084	< 2 ppm
135 (AZC521)	5.33	2.07	0.49	0.026	0.26	0.0012	< 2 ppm
100	5.21	2.3	0.49	0.03	0.27	0.0012	< 2 ppm
75	5.07	2.57	0.51	0.026	0.27	0.0011	< 2 ppm
153	4.87	2.99	0.48	0.031	0.28	0.0015	0.0024
136 (AZC531)	5.45	3.08	0.49	0.03	0.23	0.0012	< 2 ppm
66	5.59	3.18	0.54	0.026	0.25	0.0013	< 2 ppm
137 (AZC541)	5.42	4.15	0.47	0.025	0.24	0.0019	< 2 ppm
138	4.51	4.16	0.48	0.024	0.22	0.00073	< 2 ppm
Copper tolerance limit of AZ53							
65 (AZ53)	5.3	3.19	0.0077	0.028	0.25	0.0015	< 2 ppm
66	5.59	3.18	0.54	0.026	0.25	0.0013	< 2 ppm
67	5.02	3.21	1	0.025	0.24	0.0014	< 2 ppm
68	5.14	3.34	1.56	0.025	0.24	0.0012	< 2 ppm
69	5.12	3.25	2.01	0.026	0.24	0.0012	< 2 ppm
Zn influence on AM50 with 40ppm Ni							
70	5.01	0.02	0.0076	0.026	0.25	0.00063	0.0032
105	5.12	0.45	0.0043	0.027	0.28	0.001	0.0037
106	5.24	1.06	0.0043	0.028	0.27	0.0014	0.004
107	5.04	2.05	0.0044	0.027	0.27	0.0013	0.0038
81	4.73	3.08	0.0027	0.027	0.26	0.0012	0.0045
80	4.87	3.46	0.0032	0.028	0.27	0.0012	0.0034
108	5.11	4.28	0.0042	0.027	0.26	0.0015	0.0039
Ni tolerance limit of AZ53							
77	5.12	3.06	0.0033	0.027	0.27	0.0012	0.0005
78	5.04	3.63	0.0026	0.027	0.27	0.002	0.0014
79	4.89	3.17	0.0022	0.028	0.27	0.0012	0.0024
80	4.87	3.46	0.0032	0.028	0.27	0.0012	0.0034
81	4.73	3.08	0.0027	0.027	0.26	0.0012	0.0045
157	5.05	2.99	0.0029	0.019	0.24	0.00027	0.22
Galvanic coupling							
Tau(Cu), (τ(Cu))	31.8	30.65	8.88	0	0	0.014	0
Tau, (τ)	17.2	60.5	0	0	0	0	0
Beta, (ß)	41.6	0	0	0	0	0.056	0
Beta(Zn), (ß(Zn))	42.2	6.2	0	0	0	0.13	0
HP Mg	0.003	0.005	0.0001	0.001	0.003	0.006	0.0002
Mg3Al	2.93	0.002	0.0009	0.001	0.02	0.02	0.0002
Mg6Al	5.64	0.002	0.001	0.0001	0.019	0.016	0.0002

Table 2: Results of the galvanic coupling between Mg matrix with different Al content and the various samples consisting of intermetallic phases ß and τ a) average current density in μA/cm^2 b) mixed potential in mV$_{Ag/AgCl}$ after 20 h

a)

	HP Mg	Mg3Al	Mg6Al
Beta, (ß)	339	115	113
Beta(Zn), (ß(Zn))	415	244	207
Tau(Cu), (τ(Cu))	87	38	32
Tau, (τ)	102	45	30

b)

	HP Mg	Mg3Al	Mg6Al
Beta, (ß)	-1557.6	-1517.2	-1496.6
Beta(Zn), (ß(Zn))	-1557.9	-1510.8	-1507.2
Tau(Cu), (τ(Cu))	-1572.0	-1516.3	-1500.1
Tau, (τ)	-1628.4	-1518.3	-1507.9

Table 3: Phase fractions (%) for an alloy with 5 wt% Al, 0.5 wt% Mn, 0.5 wt% Cu and increasing Zn contents obtained from Scheil calculations

Phase fraction	Al_8Mn_5	Mg(Al)	$Al_{11}Mn_4$	Al_4Mn	Q	τ	ß	Φ	MgZn
AM50	0.37	95.54	0.0034	0.0020	0	0	4.08	0	0
AZC501	0.38	95.38	0.0032	0.0018	1.02	0	3.21	0	0
AZC511	0.41	94.89	0.0027	0	0.32	1.71	2.42	0.21	0.03
AZC531	0.43	93.53	0.0021	0	0	2.91	1.66	1.30	0.17
AZC551	0.43	92.08	0.0020	0.0009	0	3.54	0.78	2.82	0.33

Table 4. Calculated composition variation of phases during Scheil solidification for a magnesium alloy Mg-5Al-0.5Mn-0.5Cu-3Zn (wt%), see Fig. 3. Composition ranges correspond to decreasing temperature during contact with liquid.

Phase	wt%(Al,phase)	wt%(Cu,phase)	wt%(Mg,phase)	wt%(Mn,phase)	wt%(Zn,phase)
τ	34.7- 8.9	18.9-0	32.2- 24.0	0[a)]	14.3- 67.0
β	34.0-30.4	< 10^{-4}	53.1- 51.4	0[a)]	12.9-18.2
Φ	20.9-13.8	< 10^{-4}	40-37	0[a)]	40-50
(Mg)	1.5- 8.1[b)]	< 10^{-4}	98.1- 89.1[b)]	0.16 – 0	0.3- 6.6

a) Solubility not modeled

b) Maximum/Minimum at 391°C before β precipitates

Table 5: Tolerance limits determined for the alloy AZ53 from immersion and salt spray corrosion tests based on the results presented in Fig. 15. The composition of the tested specimens is given in Tab. 1. The tolerance limits by definition are the maximum possible impurity contents of Cu or Ni in the alloy AZ53 which can be added without exceeding the corrosion rate of the high purity AM50 (reference) in the respective corrosion test.

AZ53	immersion	salt spray
Ni	0.0022 wt%	0.0019 wt%
Cu	0.7 wt%	0.8 wt%

Table 6: Comparison of intermetallic phases and intermetallic phase compositions in the real microstructure of AZC501 and AZC531alloys

Alloy	Phase	wt% Al	wt% Cu	wt% Mg	wt% Mn	wt% Zn	wt% Fe
AZC501	τ	12 - 24	31 - 47	24 - 45	0	0	0
	β	20 - 36	0 - 8	62 - 77	0	0-2	0
	Q	30 - 34	24 - 30	35 - 47	0	0	0
	Al_8Mn_5	23 - 24	0 - 2	3 - 28	44 - 71	0	0-2
AZC531	τ	27 - 28	9 - 18	32 - 35	0	20 - 28	0
	β	27 - 29	0 - 1	53 - 55	0	17-18	0
	Al_8Mn_5	24 - 43	0	11 - 43	31 - 45	0-2	0-1

Figures

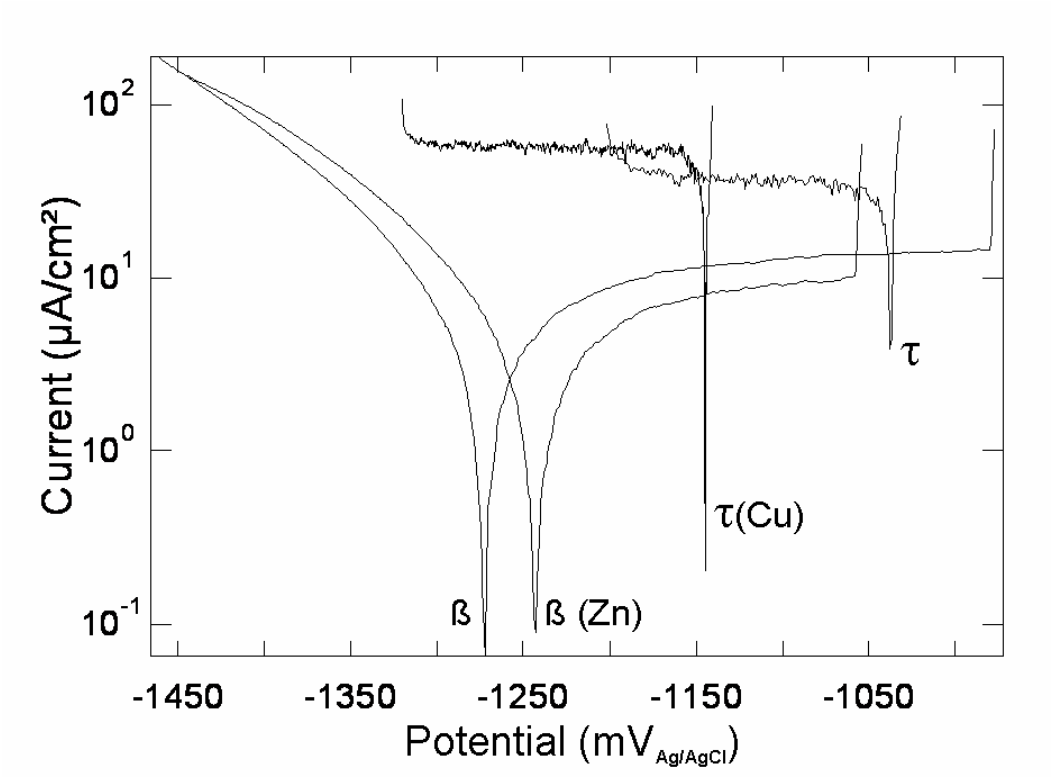

a)

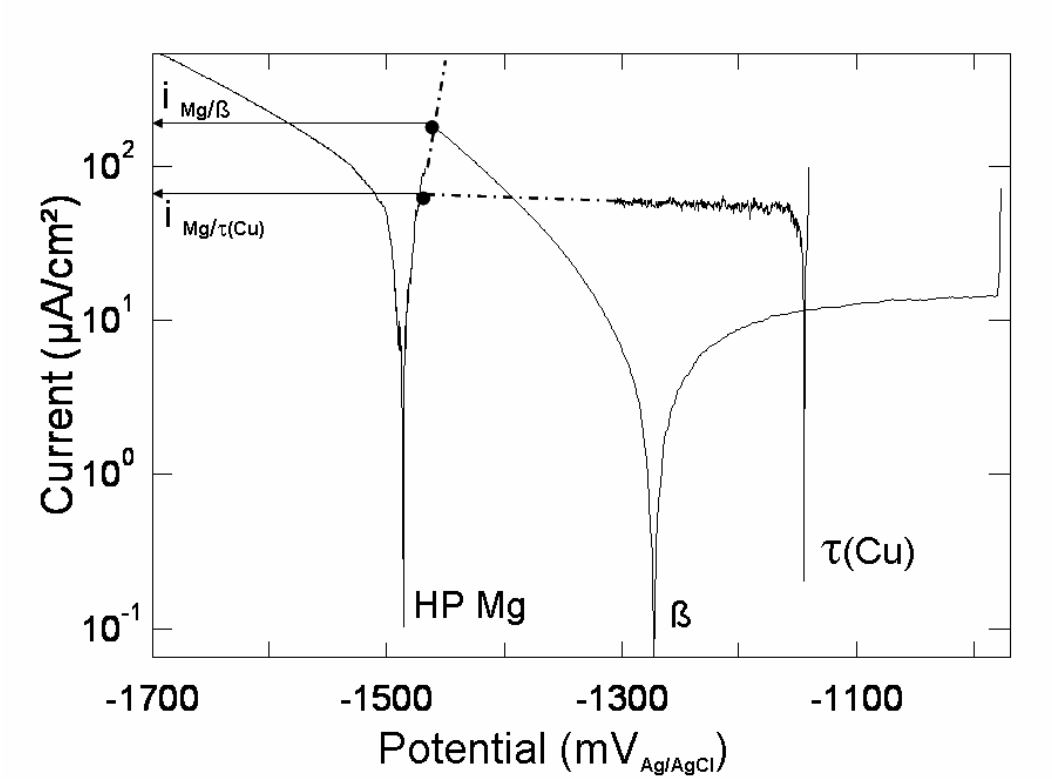

b)

Fig. 1: a) Polarisation curves of selected intermetallic phases in 5% NaCl solution (pH11), b) Estimation of the galvanic current in a possible coupling of ß and τ(Cu) with a magnesium matrix (HP-Mg), only schematic

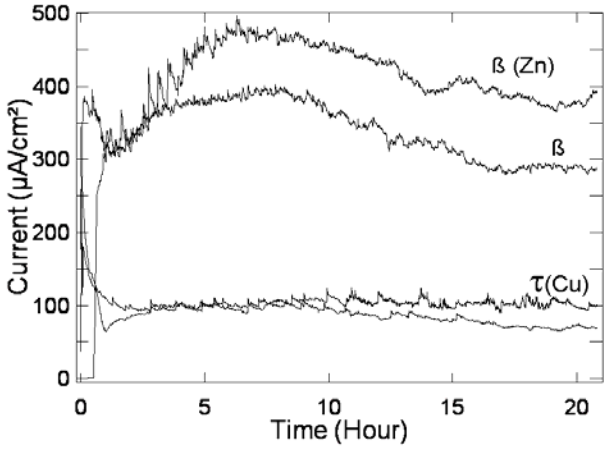

a)

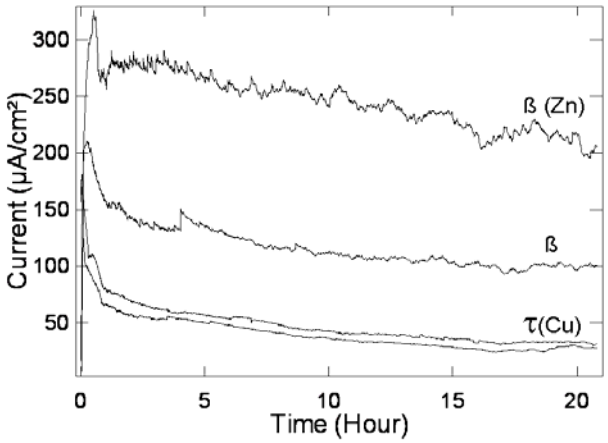

b)

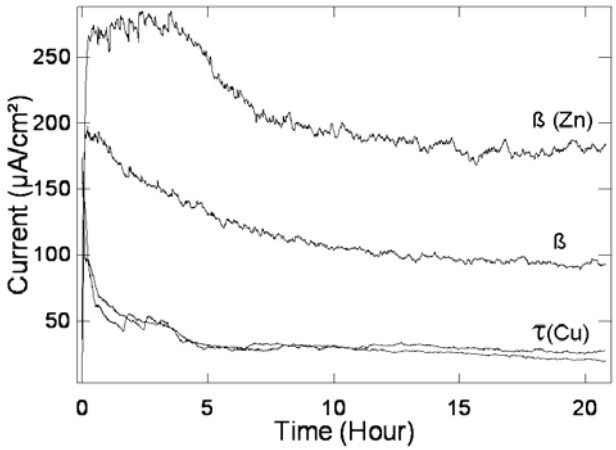

c)

Fig. 2: Current density measured during galvanic coupling between matrix and intermetallic phases in 5% NaCl solution, pH11 a) Coupling between pure magnesium and ß, ß(Zn) and τ(Cu), b) Coupling between Mg3Al and ß, ß(Zn) and τ(Cu) and c) Coupling of Mg6Al and ß, ß(Zn) and τ(Cu)

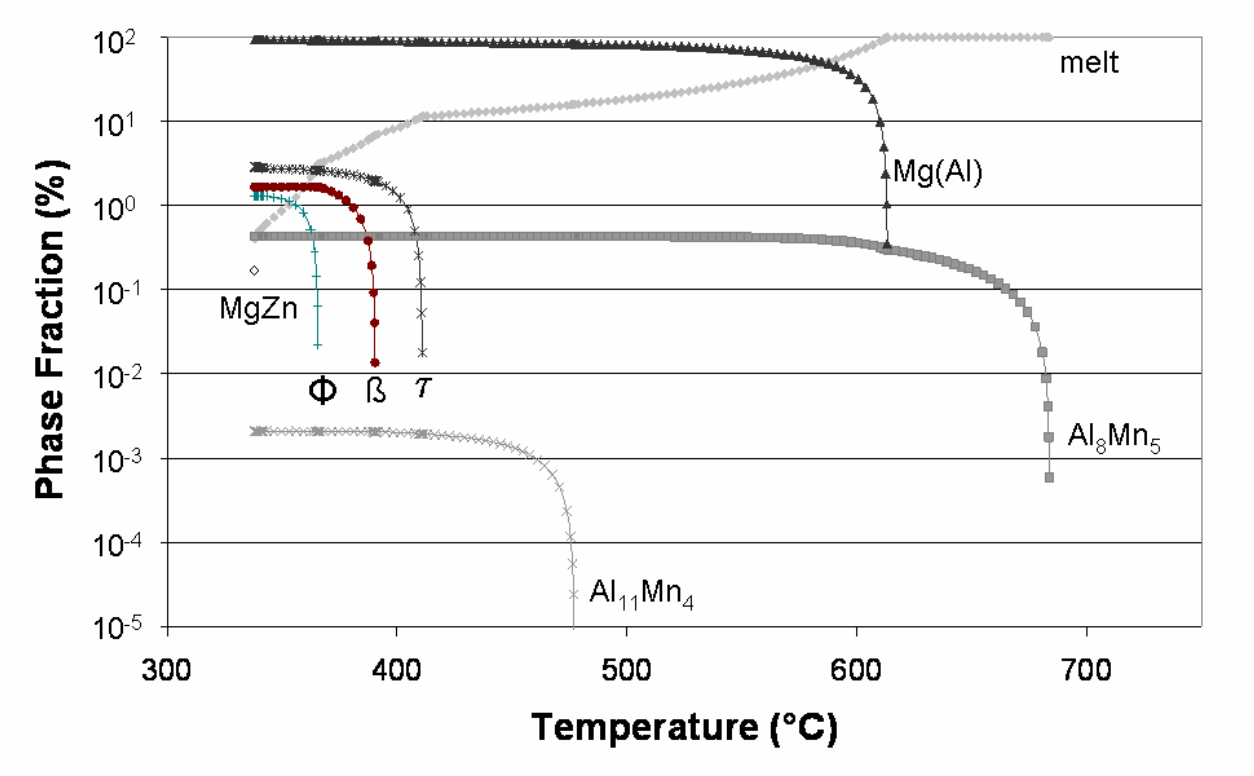

Fig. 3: Calculated phase fractions for a magnesium alloy with 5 wt% Al, 3 wt% Zn, 0.5 wt% Cu and 0.5 wt% Mn (Scheil model)

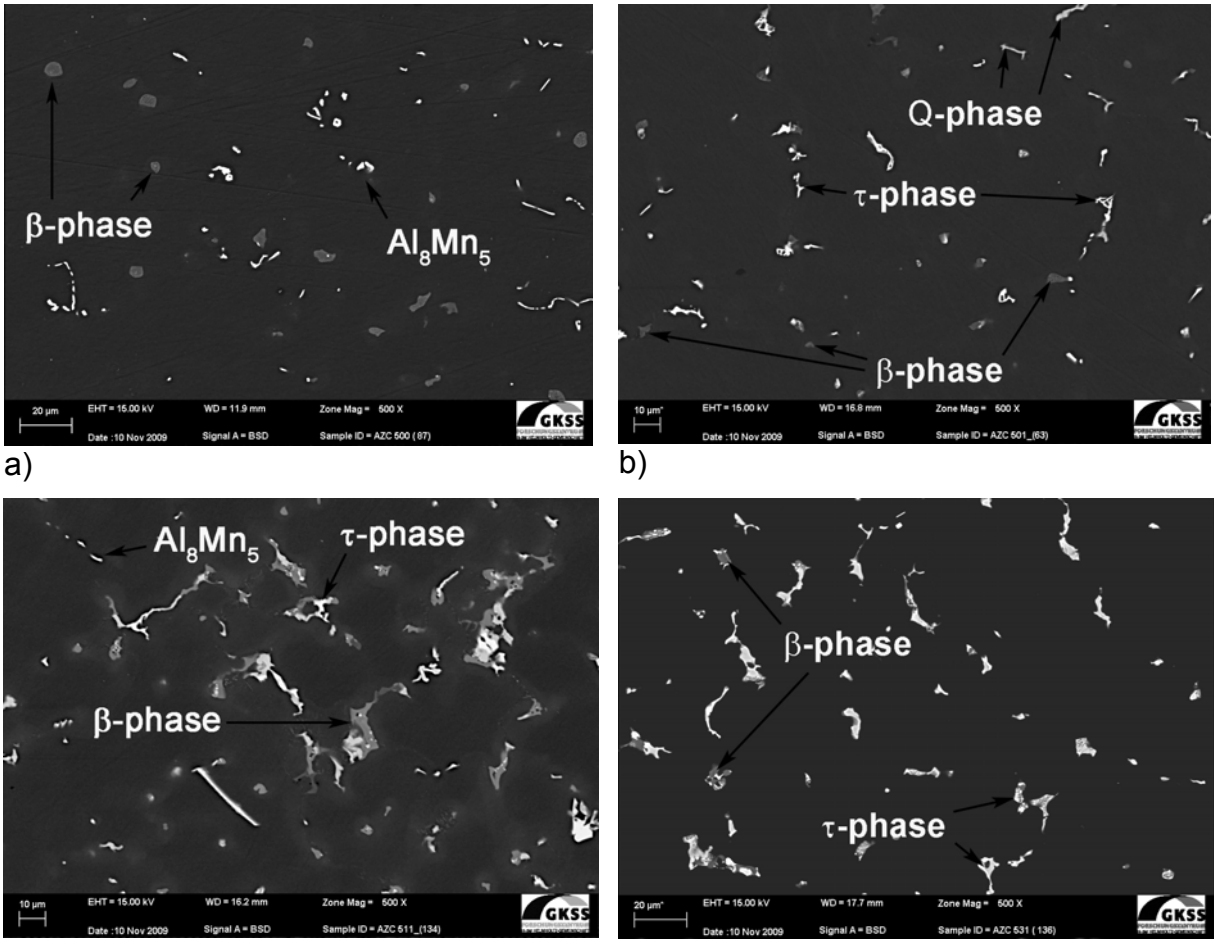

a) b)

c) d)

Fig. 4: SEM micrographs (BSE mode) showing the influence of Zn addition on the microstructure of AM50 based alloys a) AZC500 (AM50), b) AZC501, c) AZC511 and d) AZC531

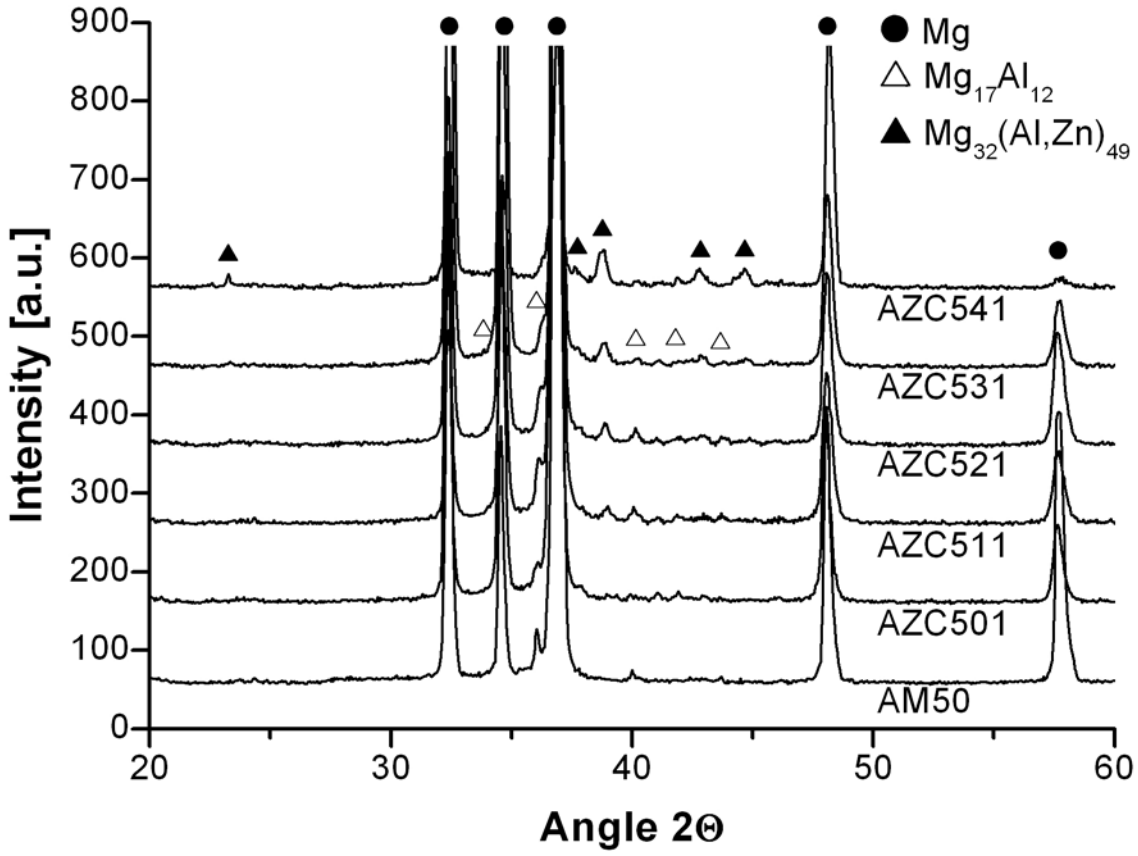

Fig. 5: XRD diffraction pattern for various AM50 based alloys with increasing Zn content

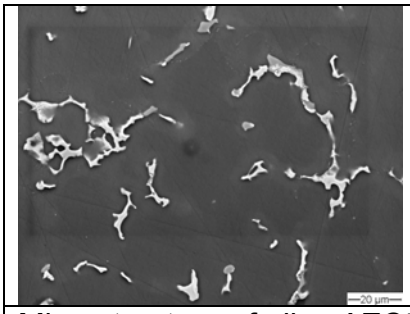

Microstructure of alloy AZC531, SEM

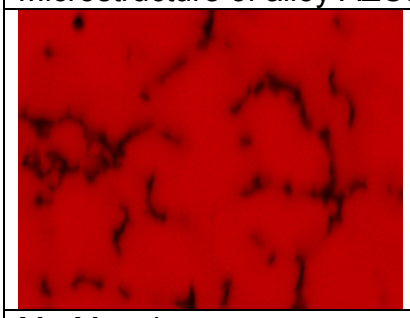

Mg-Mapping

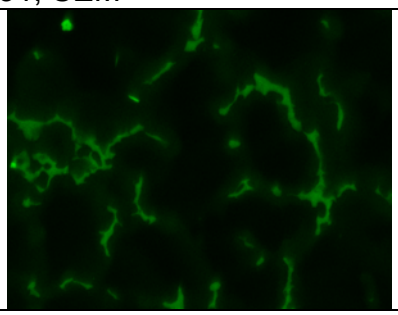

Al-Mapping

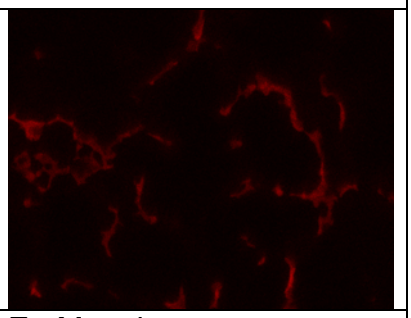

Zn-Mapping

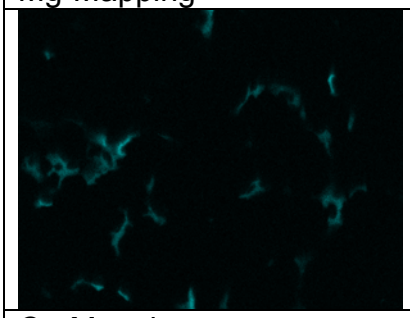

Cu-Mapping

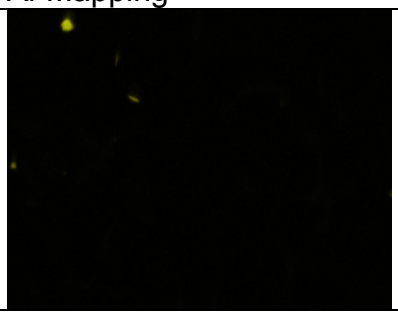

Mn-Mapping

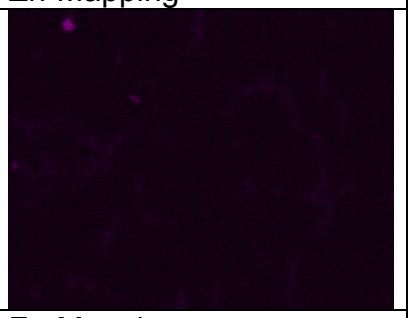

Fe-Mapping

Fig. 6: Microstructure and elemental mapping (EDX) of the elements Mg, Al, Zn, Cu, Fe and Mn revealing the distribution of each element in the different phases of an AZC531 alloy

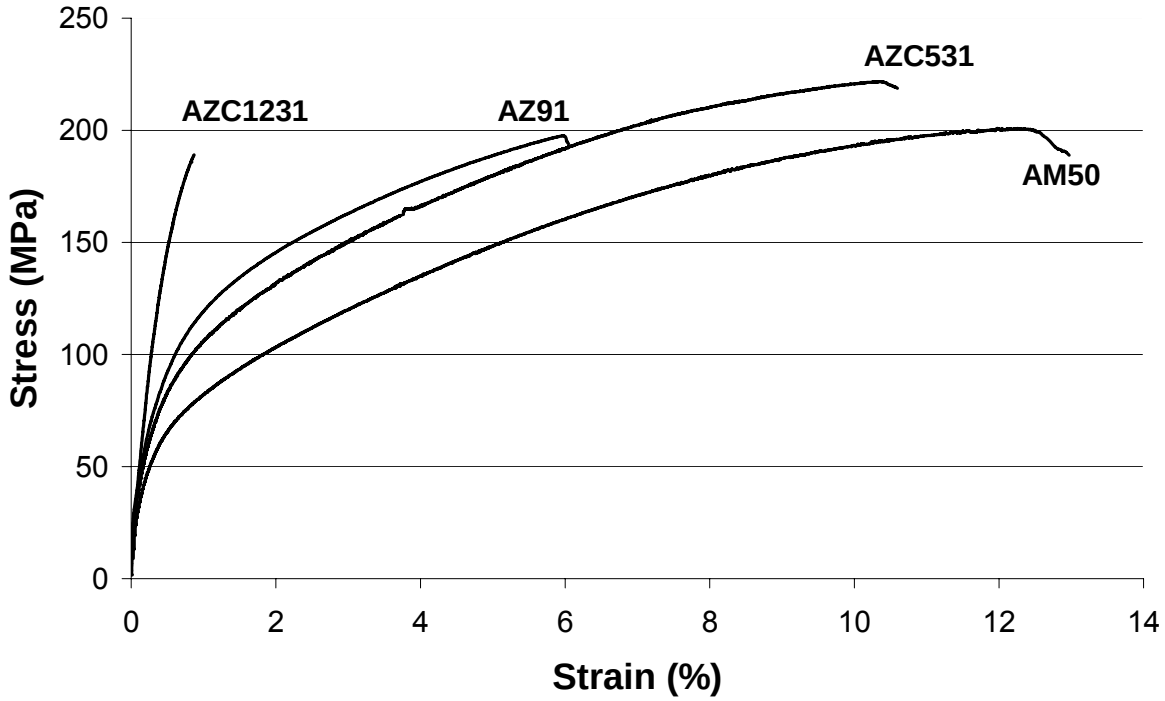

Fig.7: Comparison of the stress-strain curves of the alloys AM50, AZ91, AZC1231 and the new alloy AZC531

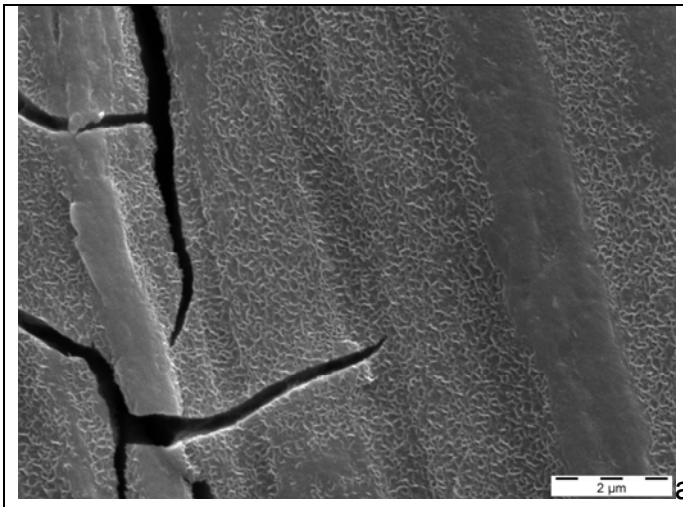

a)

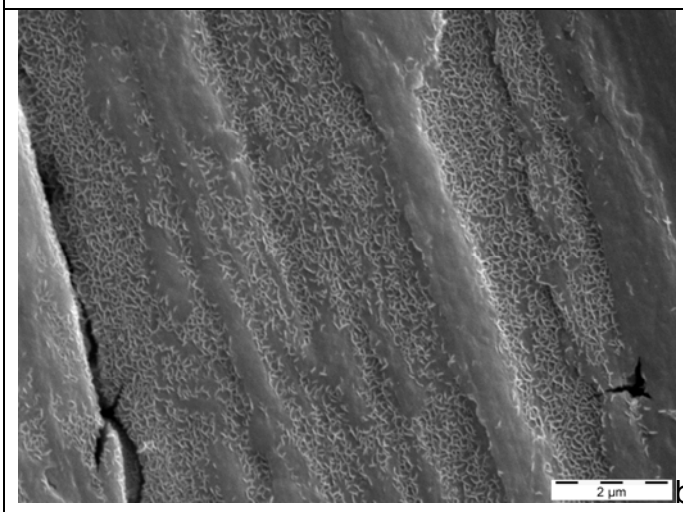

b)

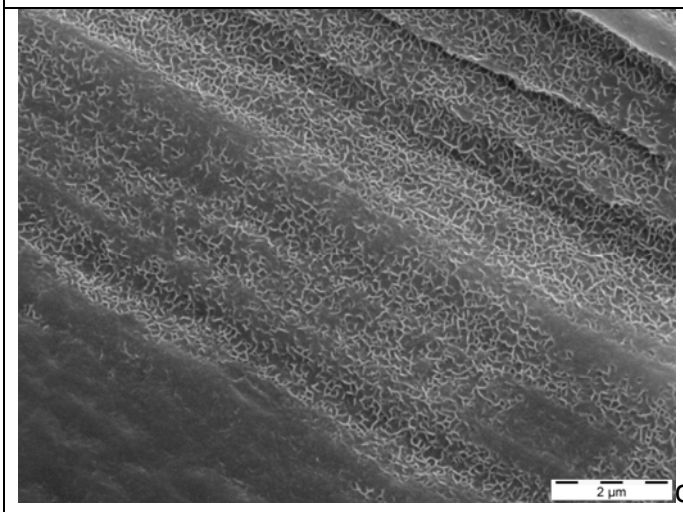

c)

Fig. 8: Comparison of the surface morphology of corroded specimens (immersion, 24 hours in de-ionised water) a) AM50 b) AZ53 and c) AZC531

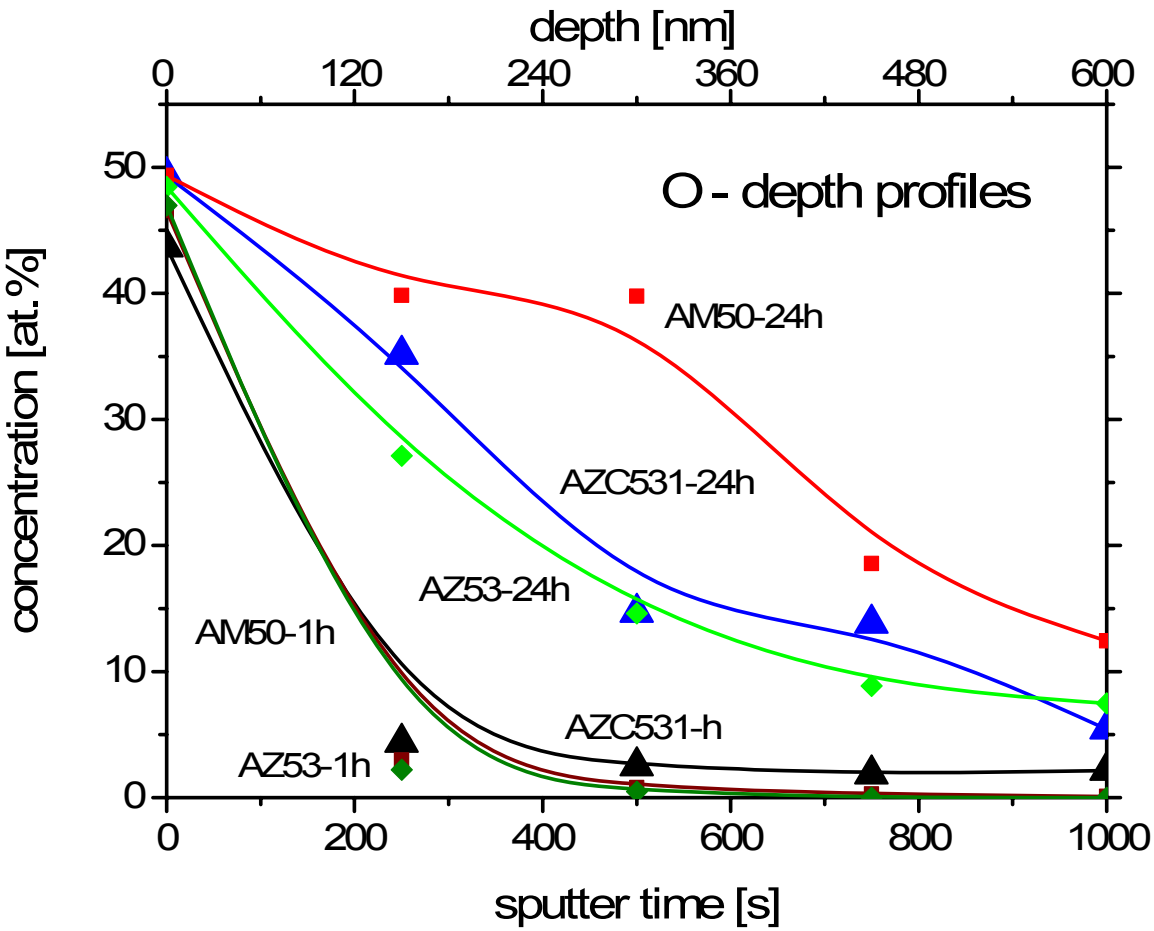

Fig. 9: Oxygen depth profiles (XPS, O 1s) on AM50, AZ53 and AZC531 specimens after immersion of 1 and 24 hours in aerated de-ionized water (the lines are only guidance for the eye).

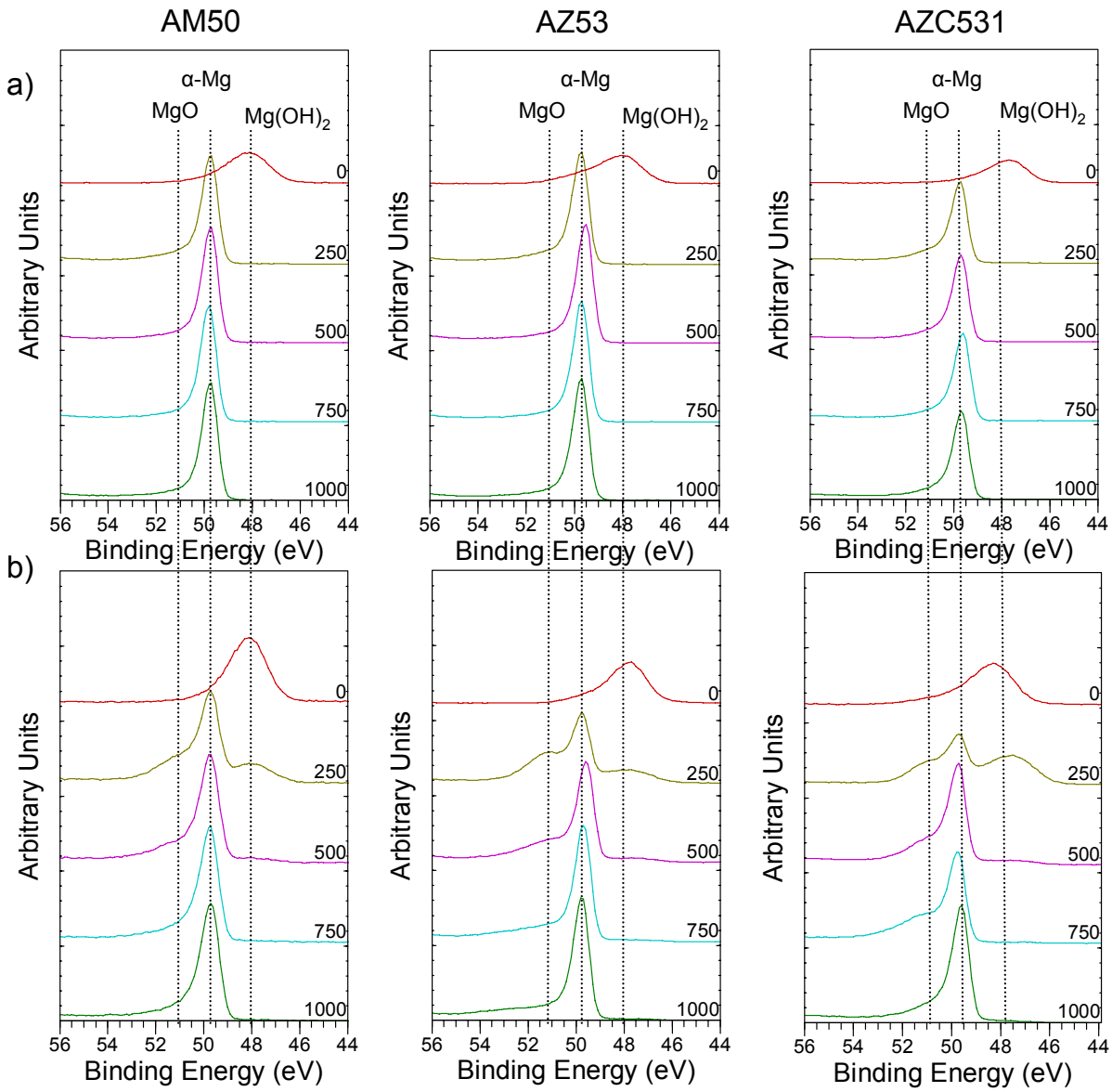

Fig. 10: XPS depth profile region scans (top=surface) of Mg 2p and detected binding states for the three alloys after a) 1hour and b) 24 hours immersion into de-ionized water

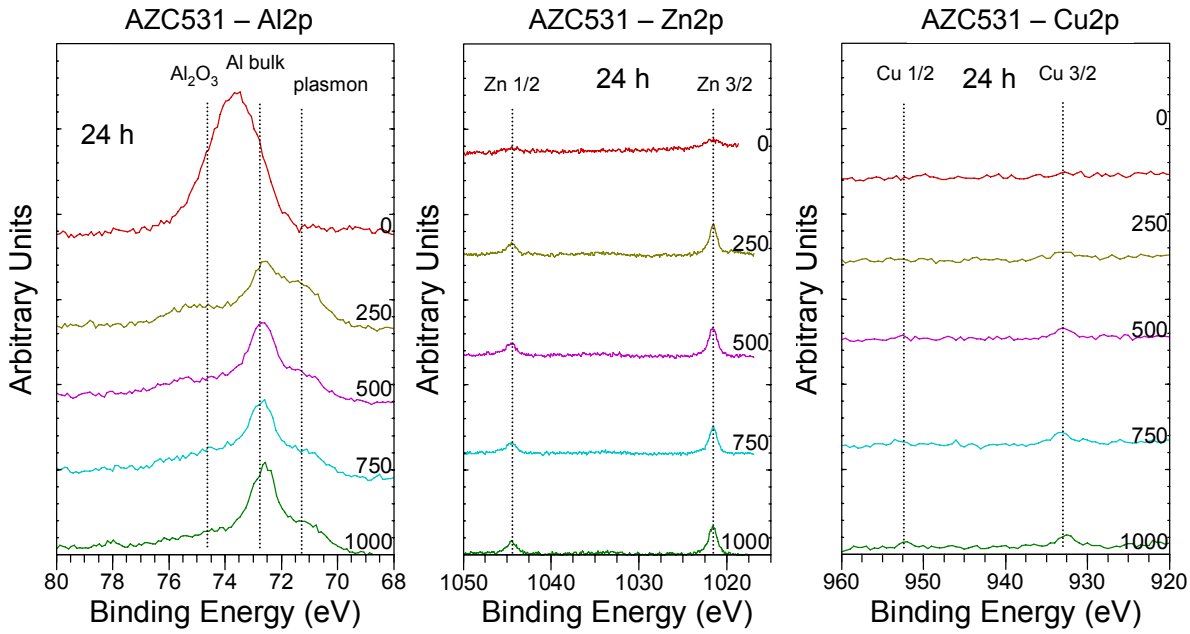

Fig. 11: XPS depth profile region scans (top=surface) of Al 2p, Zn 2p and Cu 2p (including all electron states 1/2 and 3/2) and detected binding states in the surface film of an AZC531 specimen after 24 hours immersion in de-ionized water

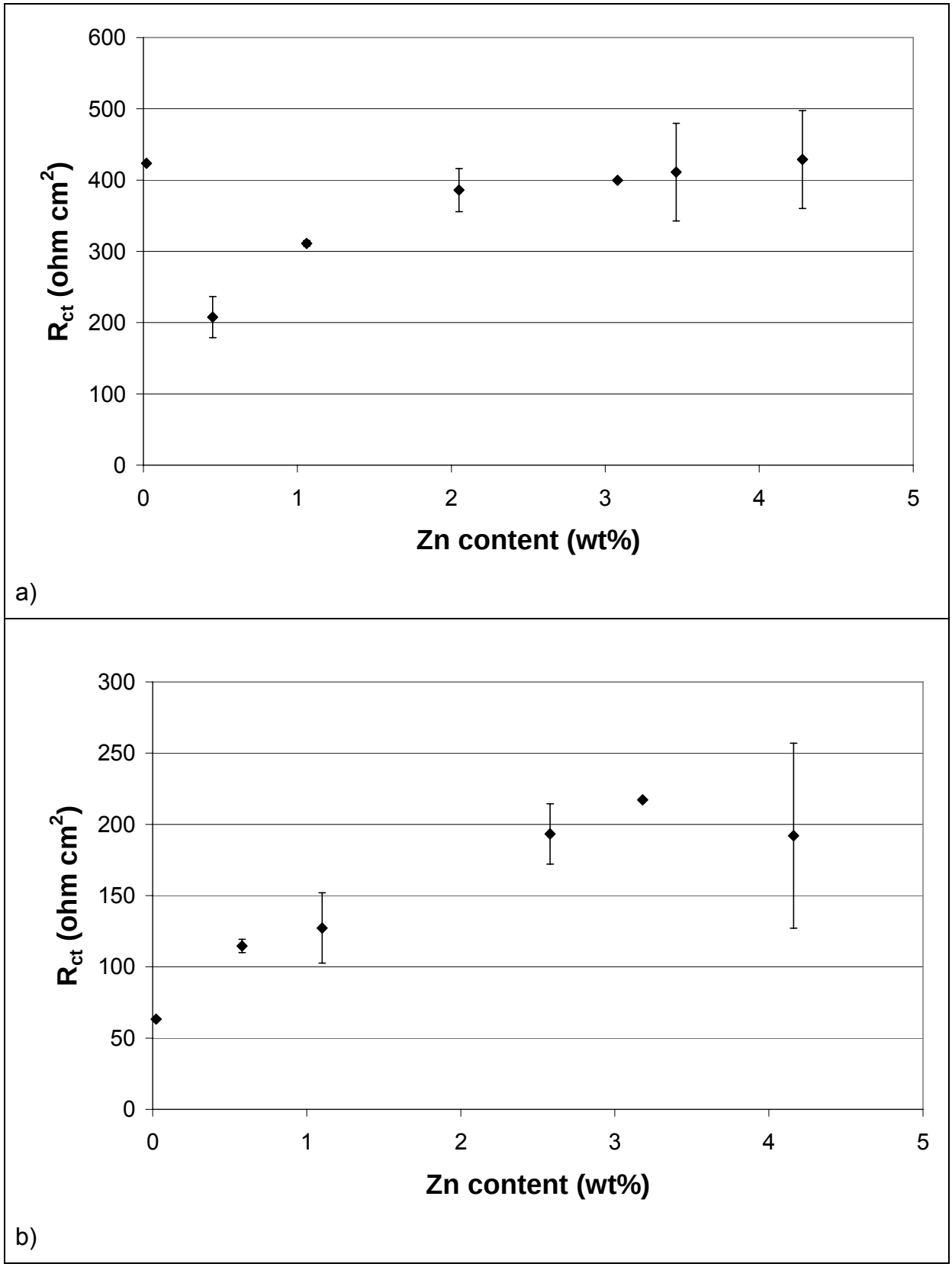

Fig. 12: Charge transfer resistance determined from EIS measurements performed on AM50 based specimens with increasing Zn content after 24 hours immersion in aqueous 5% NaCl solution a) alloys with 40 ppm Ni and b) alloys with 0.5 wt% Cu

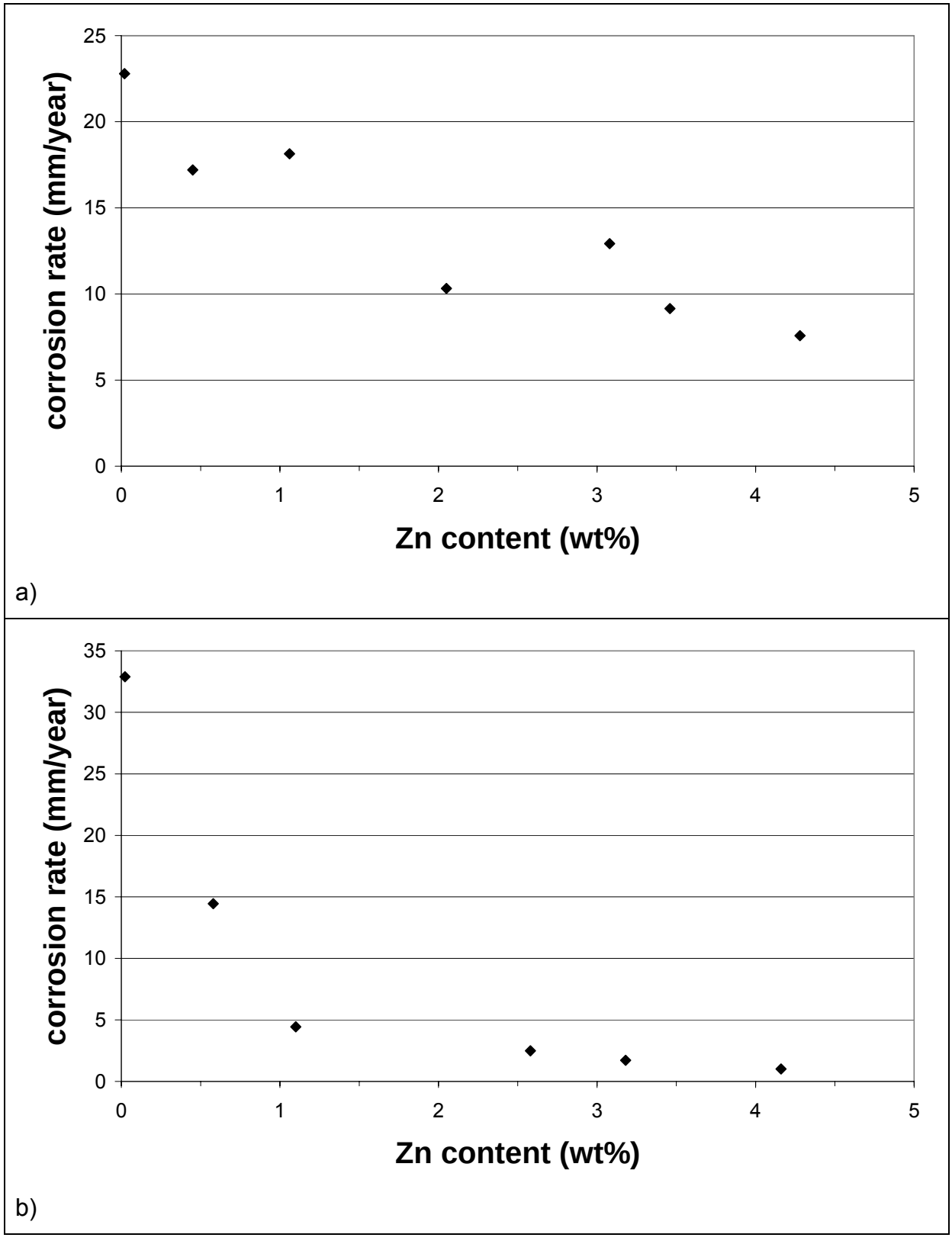

Fig. 13: Corrosion rates for AM50 based alloys with increasing Zn content determined from hydrogen evolution measurements during long term immersion tests in aqueous 3.5% NaCl solution a) alloys with 40 ppm Ni and b) alloys with 0.5 wt% Cu

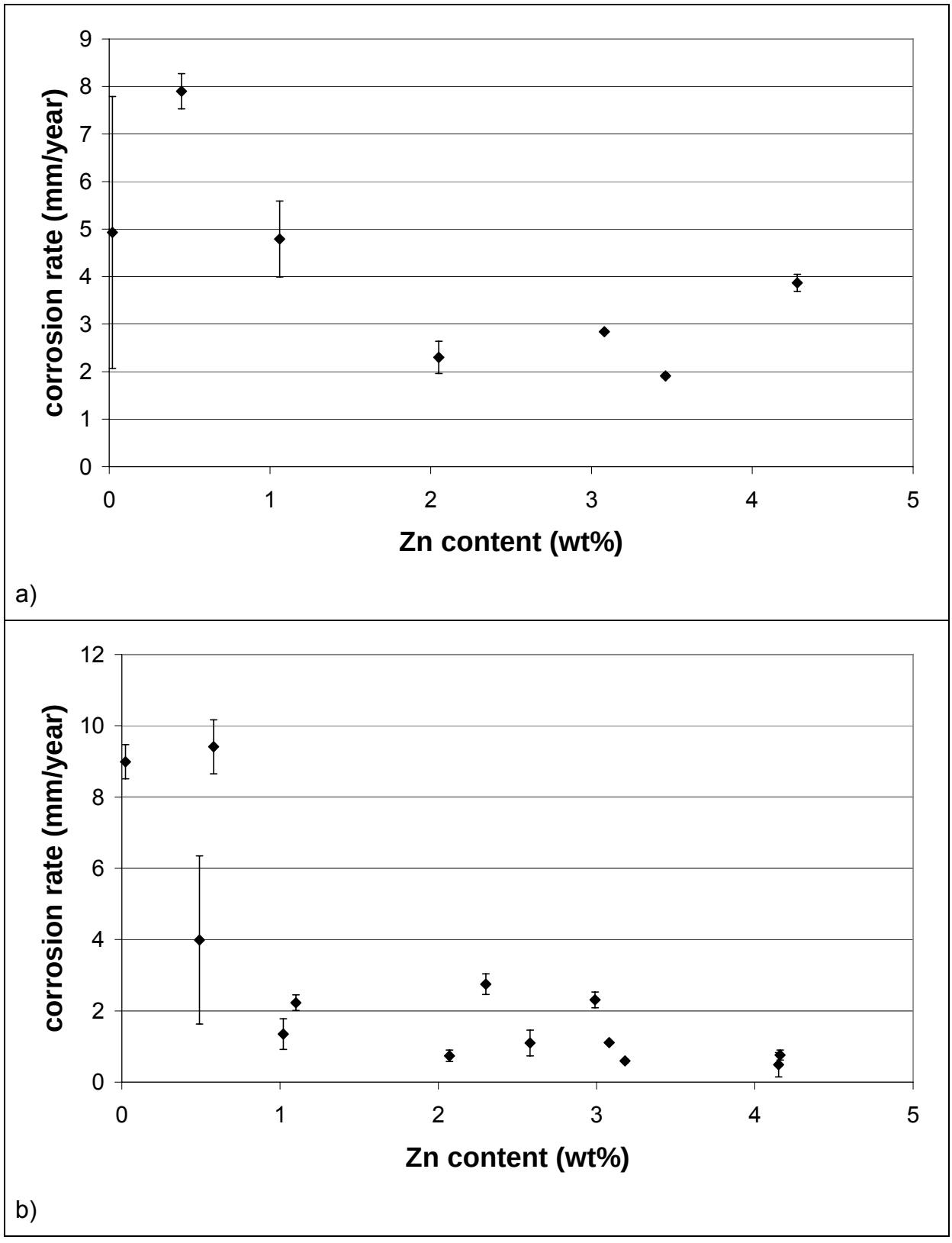

Fig. 14: Corrosion rates for AM50 based alloys with increasing Zn content determined from weight loss measurements after 48 hours salt spray testing using neutral 5% NaCl solution a) alloys with 40 ppm Ni and b) alloys with 0.5 wt% Cu

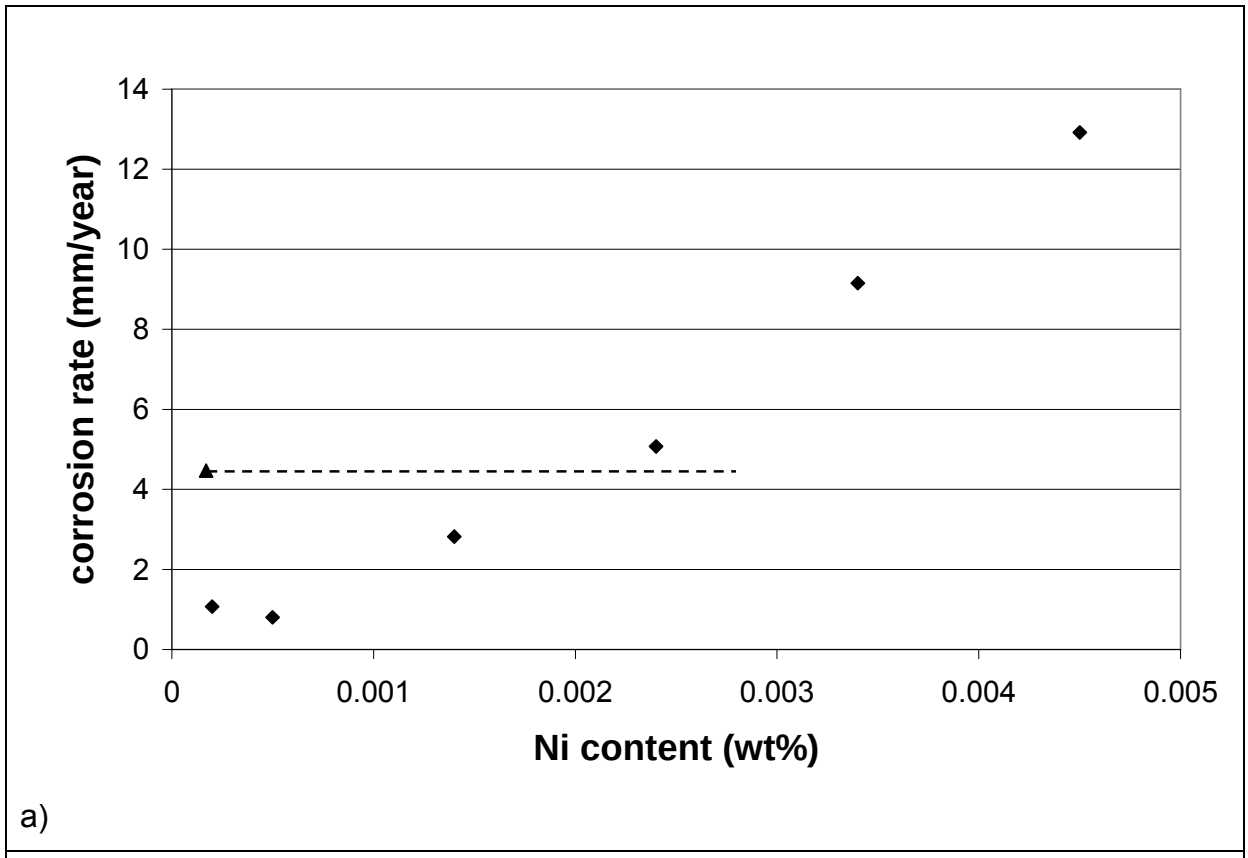
corrosion rate (mm/year)
14
12
10
8
6
4
2
0
0
0.001
0.002
0.003
0.004
0.005
Ni content (wt%)

a)

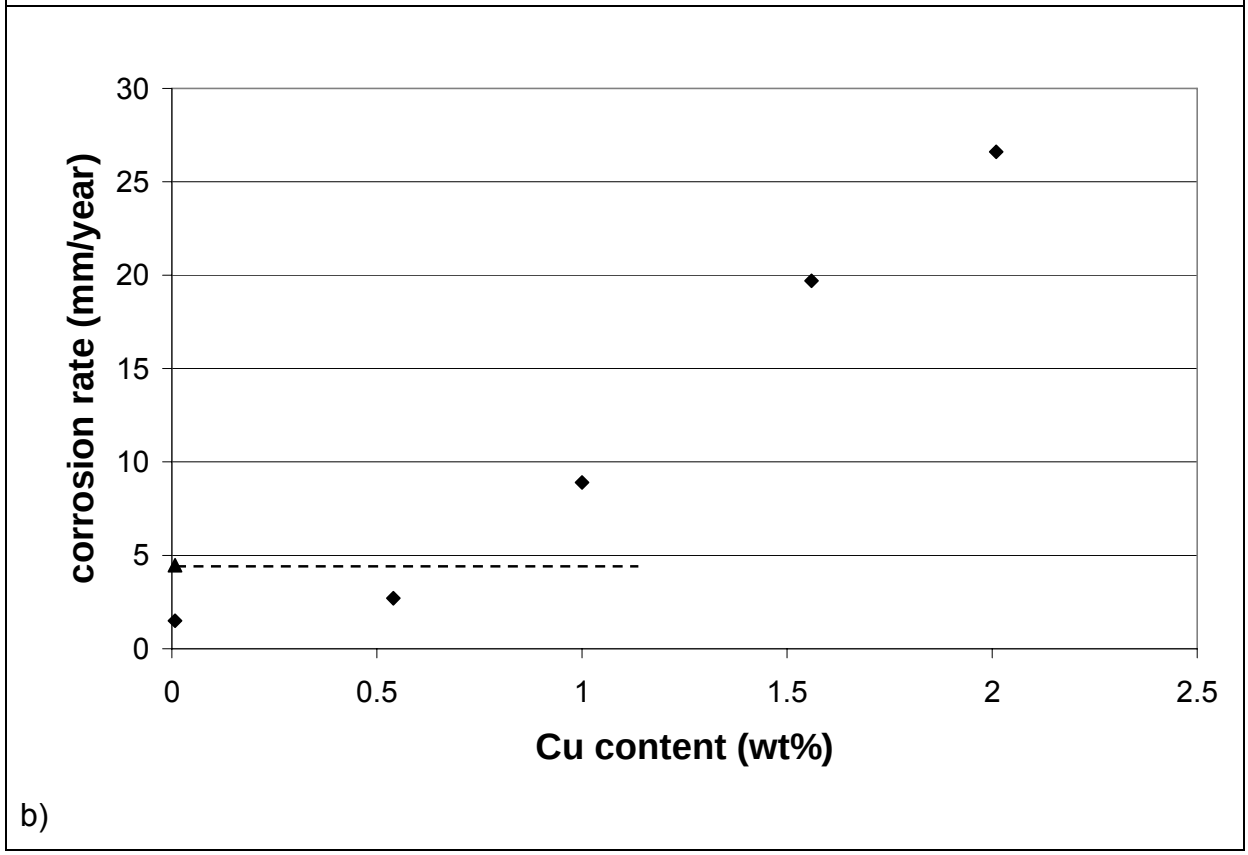
corrosion rate (mm/year)
30
25
20
15
10
5
0
0
0.5
1
1.5
2
2.5
Cu content (wt%)

b)

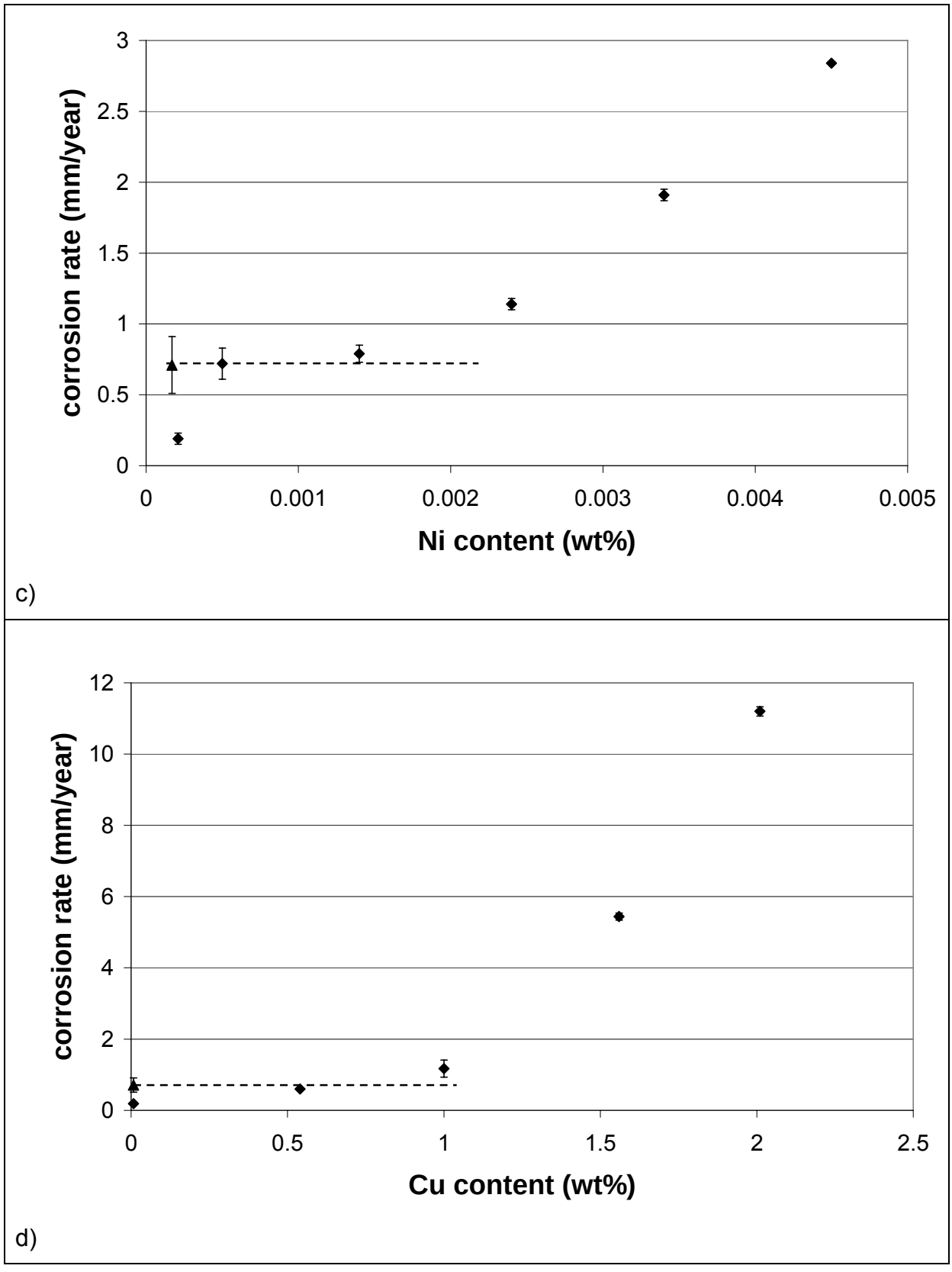

Fig. 15: Influence of impurities on the corrosion resistance of an AZ53 alloy. Tolerance limits defined by the performance of a comparable high purity AM50 alloy are marked by the dashed horizontal line. a) immersion test, 400 h, 3.5% NaCl, pH 6, nickel influence, b) immersion test, 400 h, 3.5% NaCl, pH 6, copper influence, c) salt

spray test, 48 h, 5% NaCl, pH 6.5, nickel influence, salt spray test, 48 h, 5% NaCl, pH 6.5, copper influence